VISVESVARAYA TECHNOLOGICAL UNIVERSITY

JNANASANGAMA, BELAGAVI-590018

A Project Report

on

"A Novel Approach for Detection and Localization of Landmines using Ground Penetrating Radar"

Submitted in partial fulfillment for the award of degree of

Bachelor of Engineering

In

ELECTRONICS AND COMMUNICATION ENGINEERING

Submitted by

Rajath Kumar M P   USN: 1RN12EC118

Nishanth N Bhonsle   USN: 1RN12EC096

Carried Out under the Guidance

of

Dr Vipula Singh

Professor and HOD

DEPARTMENT OF ELECTRONICS AND COMMUNICATION ENGG.

RNS INSTITUTE OF TECHNOLOGY
Channasandra, Bengaluru – 560098
2015-16

RNS INSTITUTE OF TECHNOLOGY
DEPARTMENT OF ELECTRONICS AND COMMUNICATION ENGG.
Channasandra, Bengaluru – 560098

CERTIFICATE

This is to certify that the Project entitled "**A Novel Approach for Detection and Localization of Landmines using Ground Penetrating Radar"** is a bonafide work carried out by **Rajath Kumar M P, Nishanth N Bhonsle,** bearing **USN: 1RN12EC118, 1RN12EC096** in partial fulfillment for the award of the degree of **Bachelor of Engineering** in **ELECTRONICS AND COMMUNICATION ENGINEERING affiliated** to **Visvesvaraya Technological University**, **Belagavi** during the academic year **2015-2016**. It is certified that all corrections/suggestions indicated for project have been incorporated in the report deposited in the department library. The project report has been approved as it satisfies the academic requirements with respect to project work prescribed for the **Bachelor of Engineering.**

..…………………..   ..…………………

Dr. Vipula Singh   **Dr. M K Venkatesha**

HOD and Guide   Principal

External Viva-voce

Name of the Examiners   **Signature with date**

   1.

   2.

ACKNOWLEDGEMENT

The joy and satisfaction that accompany the successful completion of any task would be incomplete without the mention of those who made it possible.

We consider ourselves proud to be a part of RNS Institute of Technology, the institution which stood by us in all our endeavors.

We express our gratitude to our beloved Chairman **Dr. R N Shetty**, for providing state of art facilities in the Institute.

We express our gratitude to **Dr. H N Shivashankar**, Director, who has always been a great source of inspiration.

We would like to express our sincere gratitude to **Dr. M K Venkatesha**, Principal, and **Dr. Vipula Singh**, Professor and HOD, Guide, for their valuable guidance and encouragement throughout our course.

Our profound gratitude to the Project coordinators, who have given us valuable suggestions and guidance throughout the project work.

We are also thankful to all the teaching and non-teaching faculty members for their constant support.

Rajath Kumar M P

Nishanth N Bhonsle

RNS INSTITUTE OF TECHNOLOGY
DEPARTMENT OF ELECTRONICS AND COMMUNICATION ENGG.
Channasandra, Bengaluru – 560098

ESTD : 2001

DECLARATION

We hereby declare that the entire work embodied in this project report titled, "**A Novel Approach for Detection and Localization of Landmines using Ground Penetrating Radar**" submitted to Visvesvaraya Technological University, Belagavi is carried out by me at Department of Electronics and Communication Engineering, RNS Institute of Technology, Bengaluru**,** under the guidance of **Dr. Vipula Singh, Professor and HOD**. This thesis has not been submitted in part or full for the award of any diploma or degree of this or any other University.

Name of the Student	USN	Signature
RAJATH KUMAR M P	**1RN12EC118**	
NISHANTH N BHONSLE	**1RN12EC096**	

ABSTRACT

An algorithm to reduce clutter and estimate the dimensions as well as material of the landmine has been proposed. Finite Difference Time Domain (FDTD) algorithm is used in order to simulate ground penetrating radar (GPR) for landmine detection. The soil is modelled considering its inhomogeneous nature and various minute anomalies which contribute as false targets. Plastic and Metal landmines have been simulated and the proposed algorithm is successful in differentiating the two. All types of possible clutter, antenna crosstalk, air-ground bounce, false target, Additive White Gaussian Noise(AWGN) and reflections have been simulated. Statistical technique, Principle Component Analysis (PCA) is used to reduce AWGN and remove false targets. A novel method to remove reflections has been proposed and discussed in detail. A correlation between the number of reflections and the material of the mine has been seen and the same has been envisaged to estimate the material. Different scenarios and real world conditions have been simulated and the proposed algorithm has been successful in detecting and classifying the mines with negligible error.

Table of Contents

III

List of Figures

CHAPTER 1

INTRODUCTION

INTRODUCTION

1.1 Ground Penetrating Radar

Ground penetrating radar (GPR) is a research tool that has many different applications. One such application is to detect the presence of land mines. It emits electromagnetic (EM) radio waves through a wideband antenna into the soil and collects the reflected signals. The principle of GPR is almost the same as in seismic wave measurement system except for the carrier signal. The propagation of electromagnetic waves in lossy materials is complex and over the past 20 years, the computational modeling of GPR has developed to improve our understanding of this phenomenon. GPR can be used in a variety of media, including rock, soil, ice, fresh water, pavements and structures. It can detect objects, changes in material, voids, cracks and other inhomogeneity.

1.2 Need For Ground Penetrating Radar

A great deal of investment is made every year by nations prone to the danger of landmines, towards the research and development of efficient methods for humanitarian demining. The idea of detecting these mines itself is extremely challenging and complex. More than 110 million anti-personal mines are estimated to be in the ground around the world. Most AP mines are small, about 60-120 mm diameter and 40-70 mm thick, and objects made of wood or plastic. The trigger mechanism in most AP mines has more negligible or no metal content and the mines are similar in size to a hockey puck. Fig 1.1 shows a few different types and shapes of landmines.

Fig 1.1 Different types of Landmines

Figure 1.2 shows a cross section of the M14 AP land mine used by U.S. army. The challenge of detecting and destroying all these devices is overwhelming. It is even more daunting when one considers the mines are still being placed in the ground faster than they can be detected and safely removed. The ideal clearance program must give confidence that all mines have been detected and cleared. GPR has a role to play in the detection process but the challenge is to translate the potential into practical system that will make a real impact on this serious humanitarian problem.
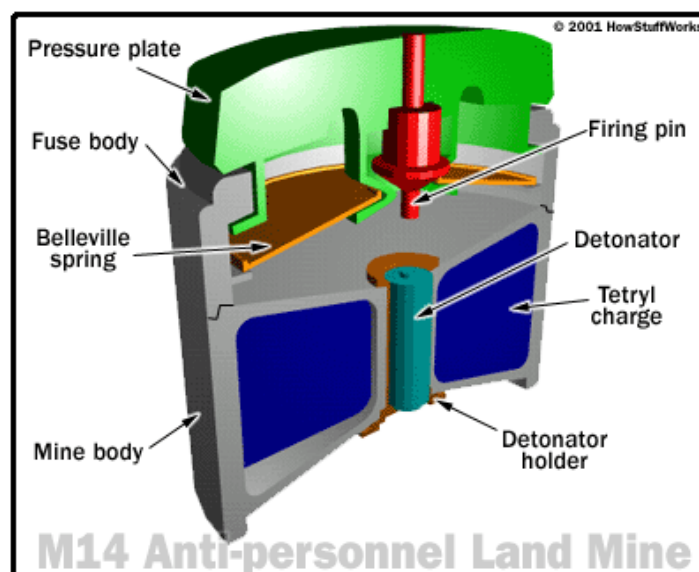
Fig 1.2 Cross section of the M14 AP Landmine

1.3 Principles of GPR

GPR has been developed over the past 30 years for shallow, high resolution investigations of the subsurface. It is a time dependent geophysical technique that can provide 3D pseudo image of subsurface, including the fourth dimension of colour and can also provide accurate depth estimates for common sub surface objects. GPR uses the principle of scattering of electromagnetic waves to locate the buried object. The basic principles and theory of operation for GPR have evolved through the disciplines of electrical engineering and seismic exploration. Practitioners of GPR tend to have back grounds either in geophysical exploration or electrical engineering. The fundamental principle of operation is the same as that used to detect aircraft overhead, but with GPR antennas are over the surface and rotate at a fixed point. This has led application of field operational principles that are analogues to the seismic reflection method.

The electromagnetic wave, radiated from the transmitting antenna, travels through the material at a velocity, determined primarily by the permittivity of the material. The wave spreads out and travels downward until it hits an object that has different electrical properties from those of surrounding medium. The wave is scattered from the object, and is detected by a receiving antenna. The surface surrounding the advancing wave is called a wave front. If the wave hits a buried object, then part of wave's energy is reflected back to the surface, while part of its energy continues to travel downward. The wave that is reflected back to the surface is captured by the receiving antenna, and recorded on a digital storage device for later interpretation.

A GPR couples EM waves to the ground and samples the mismatch echoes. An EM wave will be back scattered on any electrical parameter contrast in the ground, i.e., the permittivity ε, the permeability μ or the conductivity σ. All these three macroscopic parameters are functions of frequency. In practice, however it is the contrast in permittivity that leads to a reflection of the radiated EM waves. Earth materials are mostly nonmagnetic materials, having a relative magnetic permeability $\mu_r = \mu/\mu_0$ of 1 with $\mu_0 = 4 \times 10^{-7}$ H/m being the permeability of free space. No contrast in permeability will be encountered. The change in conductivity primarily affects absorption of the radar signal by the medium. The variation in permittivity has the largest impact on the variation of characteristic impedance of the medium, so the encountered contrast in the permittivity between materials in the ground leads to a reflection. The data recorded by GPR are

represented as a 1D, 2D or 3D dataset, denominated by the acoustic terminology A, B and C scans.

1.4 SCANNING TECHNIQUES

1.4.1. A SCAN
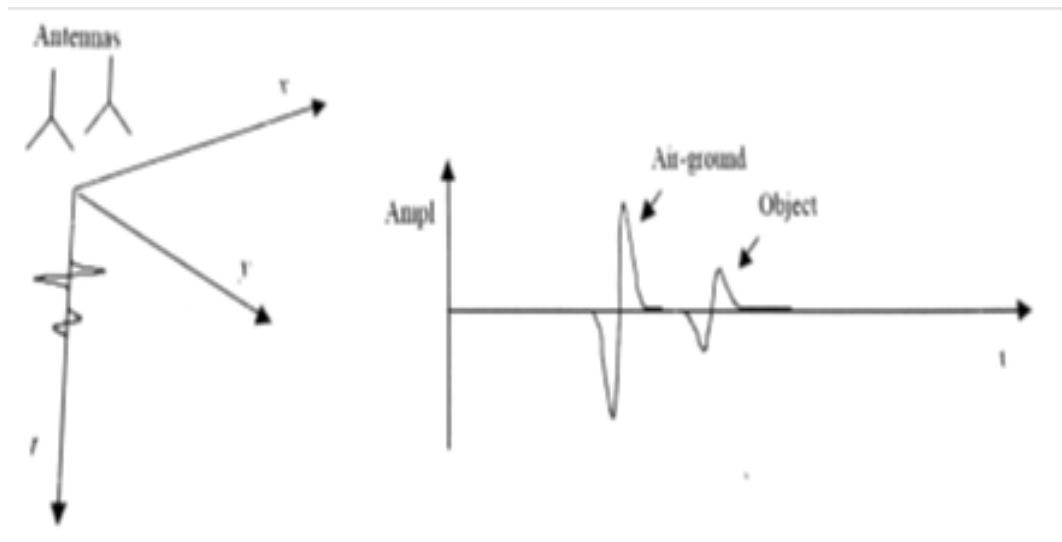
Fig 1.3 A-Scan

A single waveform b(x,y,t) recorded by a GPR, with the antennas at a given position (x,y) is referred to as an A Scan. The only variable is the time which is related to the depth by the propagation velocity of the EM waves. Figure 1.3 shows a typical A-scan.

1.4.2. B SCAN
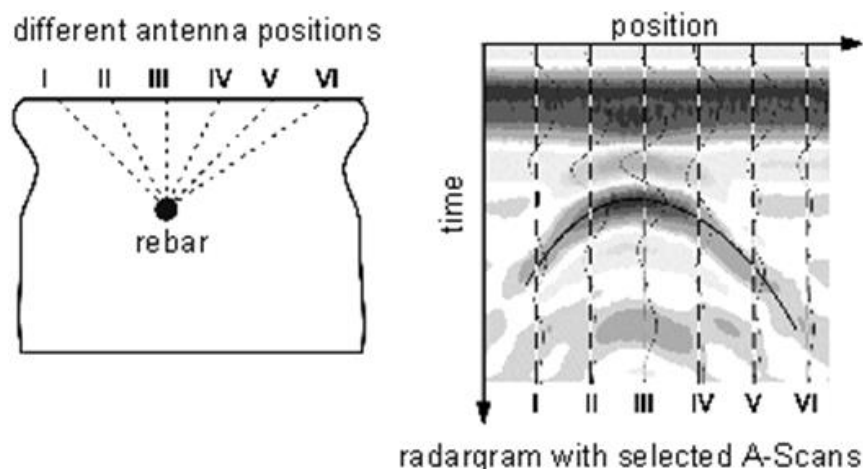
Fig 1.4 B Scan

When moving the GPR antennas on a line along the x-axis, one can gather a set of A scans, which form a 2-D data set b(x,y,t) called as B Scan. The 2-D image represents a vertical slice in the ground the time axis or related depth axis is usually pointed downwards. Figure 1.4 shows the concatenation of selected A-scans to form a B-scan (radar-gram).

1.4.3. C Scan
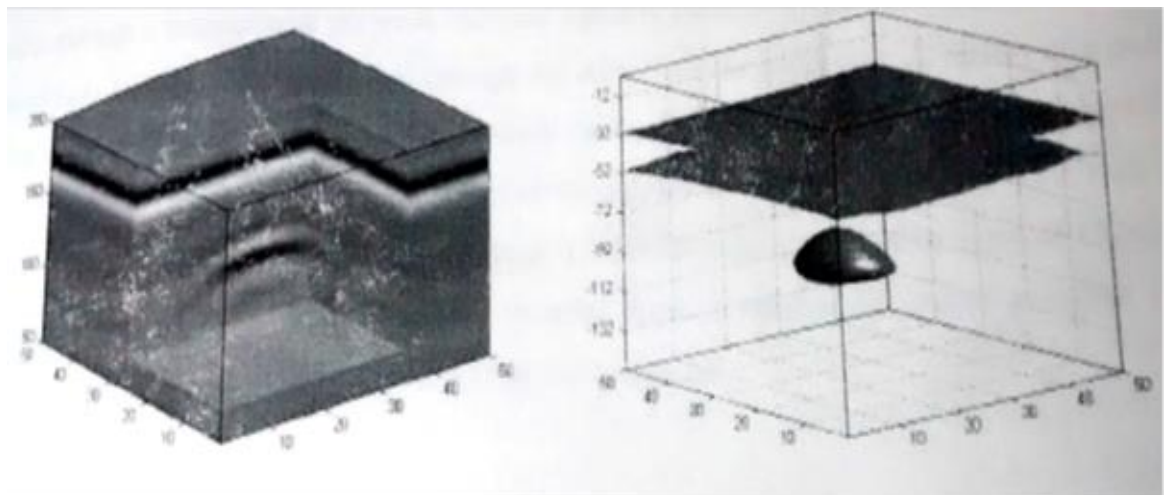
Fig. 1.5 C Scan

Finally when collecting multiple parallel B scans or in other words, when moving the antenna over a regular grid in the x y plane, a 3-D data set b(x,y,t) can be recorded, called a C Scan. Usually a C scan is represented as a 2-D image by plotting the amplitudes of the recorded data at a given time t. The image (x,y,t) represents then a horizontal slice at a certain depth . Figure 1.5 shows the stacking of B-scans to form a C-scan.

1.5. Block Diagram of GPR

GPR data records the two-way travel time using the reflections from the ground and the GPR block diagram is as shown. A signal source generates the electromagnetic wave and the EM signal is launched into the earth through a transmitter and the weak reflected signal is detected by the receiving antenna and amplified. The signal is then passed through the ADC (Analog to Digital Convertor) into the processor. A variety of signal processing algorithms can be used to process the data which can be displayed. The data is usually presented as a 2D or 3D image resembling the geometry of the subsurface,

featuring a typical GPR with a receiver span of 1m and would operate over a range 2 to 2.3 GHz for investigative depth of 150mm below soil surface. GPR data is usually recorded from a number of scans obtained by positioning the antennas along the ground. Figure 1.6 depicts the working of ground penetrating radar.
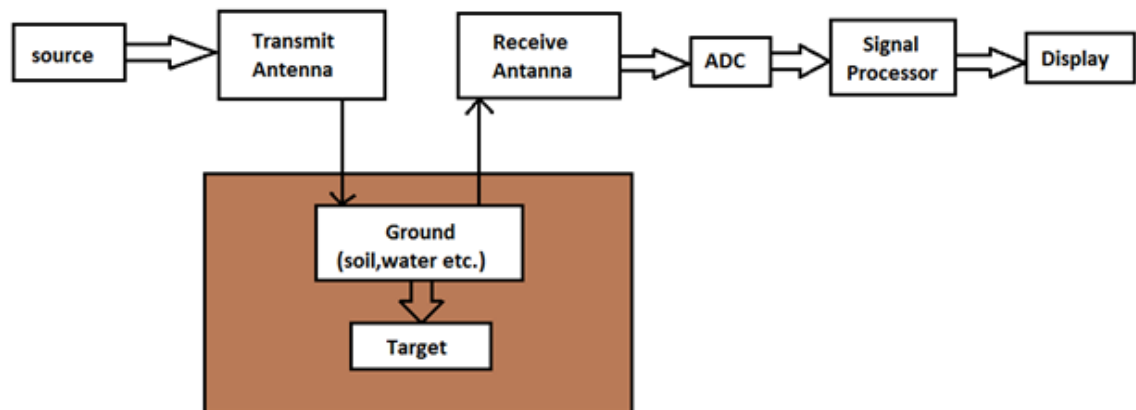
Fig 1.6 Block Diagram of GPR System

1.6. Applications of GPR

GPR is an effective tool for subsurface inspection and quality control on engineering construction projects. The numerous applications of GPR include the following:

1. Mapping pipes (including PVC pipes), cables and other buried objects.
2. Continuous inspection of layers in road pavements and airport runways. Due to the rapid data acquisition rates, it can be used at highway speeds to monitor changes in subgrade and asphalt pavement layers.
3. Mapping cavities or voids beneath road pavements, runways or behind tunnel linings.
4. To monitor the condition of railway ballast, and detect zones of clay fouling leading to track instability.
5. Detailed inspection of concrete structures, location of steel reinforcing bars and pre- and post-tensioned stressing ducts. GPR can be used in 3-D mode to map multiple layers of steel in buildings, in order to avoid damage when drilling through such structures.
6. Inspection and quality control of pre-cast concrete structures, such as bridge deck beams.
7. Detection of zones of honeycombing, voiding and chloride attack in concrete.

8. Mapping zones of deterioration and delamination on bridge decks.

9. Mapping zones of termite attack or fungal decay in trees or timber structures, such as wooden bridge beams.

10. Mapping soil, rock or fill layers in geological and geotechnical investigations, or for foundation design.

11. BH-GPR is used to detect faults and for determining the degree of fracturing of the rock mass (e.g. for investigating the structural integrity of pillars, or nuclear waste repository zones).

12. Mapping bedrock and excavation conditions along proposed cable or pipeline excavations.

13. Mapping detailed sedimentary stratigraphy, both on land and beneath rivers and lakes, particularly for pipeline crossings. (GPR will penetrate through fresh water, but is rapidly attenuated by salt water).

14. Mapping snow and ice thickness on glaciers, location of ice-core holes for climate change measurements.

1.7. Objectives

1. To numerically model the GPR and landmines in realistic scenario

2. To simulate an A-Scan using GPR

3. To generate the B-scan using A-Scans

4. To develop an algorithm for landmine detection

5. To extract the location and dimensions of the landmine

6. To determine the material of the target

1.8. Organization of Thesis

Chapter 2 explains the different approaches and methodologies that have already been implemented in the same field. It gives us an insight into the problem statement and the different techniques that can be used to tackle the problem.

Chapter 3 explains as to how the data is being generated and how the modeling is being done. It explains the FDTD technique being considered for modeling and also the different parameters considered for modeling. It also shows the generation of A-scan and B-scan using GPR. It lists the clutter classification involved in this problem statement and also explains the same.

Chapter 4 represents the block diagram of the algorithm used to solve the problem statement and also explains the same. It pictorially represents each step of the algorithm and how the processing is being done.

Chapter 5 explains the different test cases considered and how exactly the algorithm works in each case. All the parameters considered are mentioned and the results obtained using the algorithm are noted and tabulated.

CHAPTER 2

LITERATURE SURVEY

LITERATURE SURVEY

1. "The Investigation of Transmission-Line Matrix and Finite-Difference Time-Domain Methods for the Forward Problem of Ground Probing Radar" [1]. It deals with the application of the transmission line matrix and the finite-difference time-domain methods for two and three dimensional numerical modeling of ground probing radar. Two dimensional models are used to study the effects of the constitutive parameters of the subsurface to the GPR signals and the limits of horizontal and vertical resolution as well as responses from common geological targets. Three dimensional models based on these numerical techniques are used to study the GPR responses from small localized targets and the advantages and disadvantages of different orientations of the transmitting and receiving antennas.

2. "Numerical Modeling of High-Frequency Ground-Penetrating Radar Antennas" [2]. Here the development of accurate numerical models of widely-used, high-frequency commercial GPR antennas is being focused. Targets are typically located close to the surface and their responses can be coupled with the direct wave of the antenna. Most numerical simulations of GPR only include a simple excitation model and by omitting the real antenna from the model, simulations cannot accurately replicate the amplitudes and wave shapes of real GPR responses. Hence, Numerical models of a 1.5 GHz Geophysical Survey Systems, Inc. (GSSI) antenna and a 1.2 GHz MALÅ GeoScience (MALÅ) antenna have been developed and it is better visualized by using the Paraview software. The metric used to initially assess the accuracy of the antenna models was a cross-correlation of the crosstalk responses from the models with the crosstalk responses measured from the real antennas. A 98 % match between modeled and real crosstalk responses was achieved.

3. "An efficient ground penetrating radar finite-difference time-domain sub-gridding scheme and its application to the non-destructive testing of masonry arch bridges" [3]. This thesis reports on the application of ground penetrating

radar (GPR) as a non-destructive technique for the monitoring of ring separation in brick masonry arch bridges. Due to the heterogeneity of these structures, the resultant signals from the interaction between the GPR system and the bridge are often complex and hence, hard to interpret. This highlights the need to create a GPR numerical model that would allow the study of the attributes of reflected signals from various targets within the structure of the bridge. The GPR numerical analysis is undertaken using the finite-difference time-domain (FDTD) method. It is demonstrated how realistic numerical modeling of GPR using the FDTD method could greatly benefit from the implementation of sub-grids into the conventional FDTD mesh. This is particularly important when (a) parts of the computational domain need to be modeled in detail and also (b) when there are features or regions in the overall computational mesh with values of high relative permittivity supporting propagation of waves at very short wavelengths.

4. "A Realistic FDTD Numerical Modeling Framework of Ground Penetrating Radar for Landmine Detection" [4]. This paper deals with a three-dimensional (3-D) finite-difference time-domain (FDTD) algorithm used in order to simulate ground penetrating radar (GPR) for landmine detection. The validity of the modeled antennas and landmines is tested through a comparison between numerical and laboratory measurements. The modeled AP landmines are buried in a realistically simulated soil. A frequency-dependent complex electrical permittivity model is used for the dielectric properties of the soil, which relates both the velocity and the attenuation of the electromagnetic waves with the soil's bulk density, sand particles density, clay fraction, sand fraction, and volumetric water fraction. Background features like vegetation and water puddles are also included in the models and it is shown that they can affect the performance of GPR at frequencies used for landmine detection (0.5-3 GHz). It is envisaged that this modeling framework would be useful as a test bed for developing novel GPR signal processing and interpretations procedures and some preliminary results from using it in such a way are presented.

5. "Ground penetrating radar and imaging metal detector for antipersonnel mine detection" [5]. It emphasizes to concentrate on commercial impulse ground

penetrating radar with a 1 GHz antenna and a metal detector used for imaging purposes. The metal detector should help to distinguish two objects with similar radar echoes but different metal content, e.g. a mine and a stone of the same size. The GPR should in turn differentiate a mine from metallic debris, which often gives a similar metal detector answer.

6. "Finite-Difference Time-Domain Simulation of Ground Penetrating Radar on Dispersive, Inhomogeneous, and Conductive Soils" [6]. In this paper the finite-difference time-domain (FDTD) method is used to discretize the partial differential equations for time stepping of the electromagnetic fields. The soil dispersion is modeled by multi-term Lorentz and/or Debye models and incorporated into the FDTD scheme by using the piecewise-linear recursive convolution (PLRC) technique. The dispersive soil parameters are obtained by fitting the model to reported experimental data. The perfectly matched layer (PML) is extended to match dispersive media and used as an absorbing boundary condition to simulate an open space.

7. "A Novel Signal Processing Technique for Clutter Reduction in GPR Measurements of Small, Shallow Land Mines" [7]. In this paper a signal processing technique is developed to reduce clutter due to ground bounce in ground penetrating radar (GPR) measurements. This technique is especially useful when a GPR is used to detect subsurface antipersonnel mines. The GPR clutter is modeled using a simple parametric model. Buried mine and clutter contributions are separated through a pair of coupled iterative procedures.

8. "Clutter Reduction Based on Principal Component Analysis Technique for Hidden Objects Detection" [8]. It deals with the basics of Principal Component Analysis and it is used for clutter reduction in detection of hidden objects, targets hidden behind walls, buried landmines, etc. The measured data, imaged in time domain, suffer from the hyperbolic character of objects' reflections, the utilization of the Synthetic Aperture Radar (SAR) method is briefly described. The principles of ground and clutter subtraction from image are then demonstrated using training data set and SAR processed measured data.

9. "Topological Structural Analysis of Digitized Binary Images by Border Following" [9]. In this paper two border following algorithms are proposed for the topological analysis of digitized binary images. The first one determines the surroundedness relations among the borders of a binary image. Since the outer borders and the hole borders have a one-to-one correspondence to the connected components of l-pixels and to the holes, respectively, the algorithm yields a representation of a binary image, from which one can extract some sort of features without reconstructing the image. The second algorithm, which is a modified version of the first, follows only the outermost borders.

CHAPTER 3

DATA GENERATION

DATA GENERATION

3.1. Software Used

3.1.1. GprMax

GprMax is free software that simulates electromagnetic wave propagation. It solves Maxwell's equations in 3D using the Finite-Difference Time-Domain (FDTD) method. GprMax was designed for modeling Ground Penetrating Radar (GPR) but can also be used to model electromagnetic wave propagation for many other applications.

GprMax was originally developed in 1996 by Antonis Giannopoulos when numerical modeling using the FDTD method and, in general, the numerical modeling of Ground-Penetrating Radar (GPR) were in their infancy.

GprMax is released under the GNU General Public License v3 or higher. GprMax is written in Python and includes performance-critical parts written in Cython/OpenMP.

3.1.2. Paraview

Paraview which is an open source visualization application which uses the Visualization Toolkit (VTK)—with GprMax3D—electromagnetic simulation software based on the Finite-Difference Time-Domain (FDTD) method to visualize the model in 3D.

3.2. Basic Concepts of FDTD

Finite-difference time-domain or Yee's method is a numerical analysis technique used for modeling computational electrodynamics (finding approximate solutions to the associated system of differential equations). Since it is a time-domain method, FDTD solutions can cover a wide frequency range with a single simulation run, and treat nonlinear material properties in a natural way.

The FDTD method belongs in the general class of grid-based differential numerical modeling methods (finite difference methods). The time-dependent

Maxwell's equations (in partial differential form) are discretized using central-difference approximations to the space and time partial derivatives.

The finite-difference time-domain (FDTD) method is arguably the simplest, both conceptually and in terms of implementation, of the full-wave techniques used to solve problems in electromagnetics. It can accurately tackle a wide range of problems. The FDTD method is used to discretize the partial differential equations for time stepping of the electromagnetic fields.

All electromagnetic phenomena, on a macroscopic scale, are described by the well-known Maxwell's equations. These are first order partial differential equations which express the relations between the fundamental electromagnetic field quantities and their dependence on their sources. The equations are:

$$\nabla \times E = -\frac{\partial B}{\partial t}$$

$$\nabla \times H = \frac{\partial D}{\partial t} + J_c + J_s$$

$$\nabla \cdot B = 0$$

$$\nabla \cdot D = q_v$$

Where t is time (seconds) and q_v is the volume electric charge density (coulombs/cubic metre). In Maxwell's equations, the field vectors are assumed to be single-valued, bounded, continuous functions of position and time. In order to simulate the GPR response from a particular target or set of targets the above equations have to be solved subject to the geometry of the problem and the initial conditions.

The nature of the GPR forward problem classifies it as an initial value – open boundary problem. This means that in order to obtain a solution one has to define an initial condition (i.e. excitation of the GPR transmitting antenna) and allow for the resulting fields to propagate through space reaching a zero value at infinity since there is no specific boundary which limits the problem's geometry and where the electromagnetic fields can take a predetermined value. Although the first part is easy to accommodate (i.e. specification of the source), the second part cannot be easily tackled using a finite computational space.

The FDTD approach to the numerical solution of Maxwell's equations is to discretize both the space and time continua. Thus the discretization spatialΔx, Δy and Δz and temporal Δt steps play a very significant role – since the smaller they are the closer the FDTD model is to a real representation of the problem. However, the values of the discretization steps always have to be finite, since computers have a limited amount of storage and finite processing speed. Hence, the FDTD model represents a discretized version of the real problem and is of limited size. The building block of this discretized FDTD grid is the Yee cell named after Kane Yee who pioneered the FDTD method. This is illustrated for the 3D case in Fig. 3.1.

By assigning appropriate constitutive parameters to the locations of the electromagnetic field components, complex shaped targets can be included easily in the models. However, objects with curved boundaries are represented using a staircase approximation.

The numerical solution is obtained directly in the time domain by using a discretized version of Maxwell's curl equations which are applied in each FDTD cell. Since these equations are discretized in both space and time, the solution is obtained in an iterative fashion. In each iteration the electromagnetic fields advance (propagate) in the FDTD grid and each iteration corresponds to an elapsed simulated time of one dt. Hence by specifying the number of iterations we can instruct the FDTD solver to simulate the fields for a given time window.

The price we have to pay for obtaining a solution directly in the time domain using the FDTD method is that the values of Δx, Δy, Δz and Δt cannot be assigned independently. FDTD is a conditionally stable numerical process. The stability condition is known as the CFL condition after the initials of Courant, Freidrichs and Lewy and is given by,

$$\Delta t \leq \frac{1}{c\sqrt{\left(\frac{1}{\Delta x^2} + \frac{1}{\Delta y^2} + \frac{1}{\Delta z^2}\right)}}$$

Where c is the speed of light and hence Δt is bounded by the values of Δx, Δy and Δz. The stability condition for the 2D case is easily obtained by letting $\Delta z \longrightarrow \infty$.
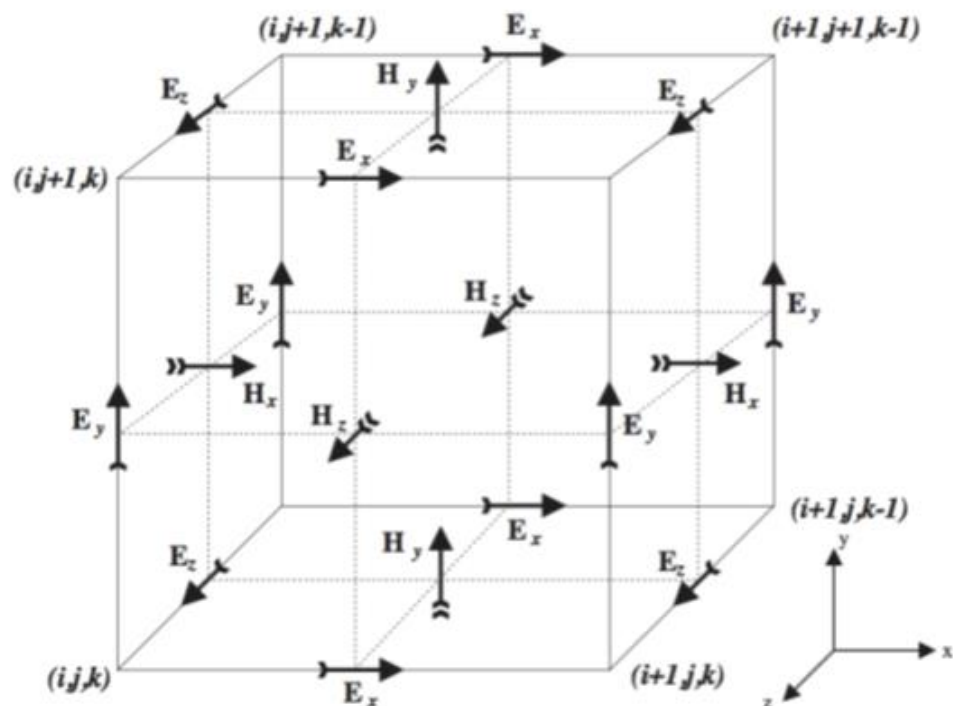
Fig. 3.1 3D FDTD Yee cell

One of the most challenging issues in modeling open boundary problems, such as GPR, is the truncation of the computational domain at a finite distance from sources and targets where the values of the electromagnetic fields cannot be calculated directly by the numerical method applied inside the model. Hence, an approximate condition known as absorbing boundary condition (ABC) is applied at a sufficient distance from the source to truncate and therefore limit the computational space. The role of this ABC is to absorb any waves impinging on it, hence simulating an unbounded space. The computational space (i.e the model) limited by the ABCs should contain all important features of the model such as sources and output points and targets. Fig 3.2 illustrates this basic difference between the problem to be modeled and the actual FDTD modeled space. It is assumed that the half-space which contains the target(s) is of infinite extent. Therefore, the only reflected waves will be the ones originating from the target. In cases where the host medium is not of infinite extent (e.g. a finite concrete slab) the assumption of infinite extent can be made as far as the actual reflections from the slab termination are not of interest or its actual size is large enough that any reflected waves which will originate at its termination will not affect the solution for the required time window. In general, any

objects that span the size of the computational domain (i.e. model) are assumed to extend to infinity. The only reflections which will originate from their termination at the truncation boundaries of the model are due to imperfections of the ABCs and in general are of very small amplitude compared with the reflections from target(s) inside the model. All other boundary conditions which apply at interfaces between different media in the FDTD model are automatically enforced in gprMax.
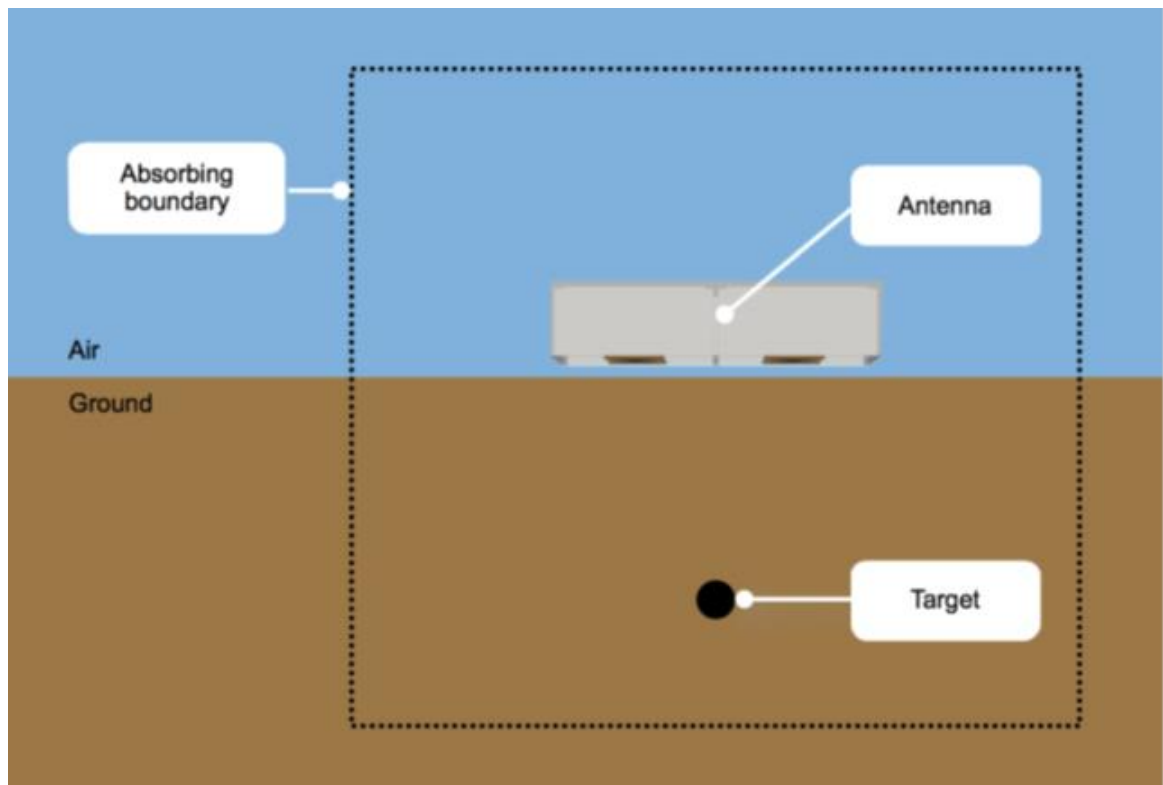
Fig. 3.2 GPR forward problem showing computational domain bounded by Absorbing Boundary Conditions (ABCs)

3.3.   Numerical Modeling

Numerical modeling techniques are directly related to the advent of the digital computer and the rapid advancements in the relevant technologies which resulted in a substantial and continuing increase in the available computational power. Computation is an essential part of the general modeling process, numbers produced by a computer program do not convey any information by themselves, unless they are part of a rational procedure which describes a physical phenomenon. The construction of a numerical model for the solution of a particular electromagnetic problem can be divided into five steps:

1. Conceptualization: The process of describing the problem in terms of physical principles in a simple form.

2. Formulation: The process of transformation of the physical principles into a more comprehensive, formal mathematical representation.

3. Numerical implementation: The step in which a computer algorithm is constructed from the mathematical representation with the aid of numerical techniques.

4. Computation: The outcome of the numerical implementation after execution as a computer program.

5. Validation: The process of verification of the output for physical reasonableness having in mind the complexity of the problem.

The different parameters considered in numerical modeling here are:

3.3.1. Domain

Domain is the size of the model where the antennas and landmines can be modeled. For example, if the domain size is 6m x 2m then all the source, receiver, landmine and other possible components should exist within the 6m x 2m boundary, failing which the components will not have any effect during simulation.

3.3.2. Time Window

It is the total time required for one simulation/scan. i.e. if time window is 7.2ns, then while simulating to generate a B-scan the time taken by the source to emit the next signal and proceed to the next step is 7.2ns, if the target/component is struck by the signal and the reflected signal traverses back to the receiver within this time domain then that particular change in voltage levels caused by that target will be detected.

3.3.3. Time Step

As explained in section [3.2] Basic concepts of FDTD, The Courant, Freidrichs and Lewy (CFL) condition is a very important consideration to check for stability. For this project, our yee cell size is 0.002m * 0.002m and it is a 2D

model thus delta z does not exist. The yee cell for all the models considered in this project remains the same. Hence the time step also remains the same throughout.

3.3.4. Material

The type of material has to be specified for every model, for this project the properties of the material that were considered to model a component are:

1. relative permittivity, ϵr
2. conductivity (Siemens/metre), σ
3. relative permeability, μr
4. magnetic loss (Ohms/metre), σ

3.3.5. Waveform

The type of waveform the source emits is also considered during modeling as the behavior of the waveform varies during reflection, caused due to the components in the domain. Two different waveforms, sine and ricker were considered for simulation. Here, step waveform was used but either step or continuous waveforms can be used.

3.3.5 Shape

Different geometrical shapes have to be considered while modeling. The shapes that were considered are spherical, cylindrical, cube and cuboid.

Example Model

In this example, the parameters that were considered are as follows:

1. Domain size is 6m x 2m
2. Time window is 7.2ns
3. Material indicated by blue color in the model has relative permittivity(6), conductivity(0.001), relative permeability(1), magnetic loss(0.001)
4. Material indicated by blue color is a perfect electric conductor
5. Ricker waveform with amplitude 1, frequency 1.5GHz and time step 4.717 pico seconds is used

6. Hertzian dipole antennas are being used for transmission and reception purpose and are kept at a distance of 1.80m from the bottom of the domain. The ground starts from 1.70m which is evident from the model

7. The antennas are moved in steps of 0.01m after each transmission and reception

8. The dimensions of the target modeled is 20x10 and the corners of the target lies at a distance of 1.4m and 1.5m as shown in the Figure 3.3
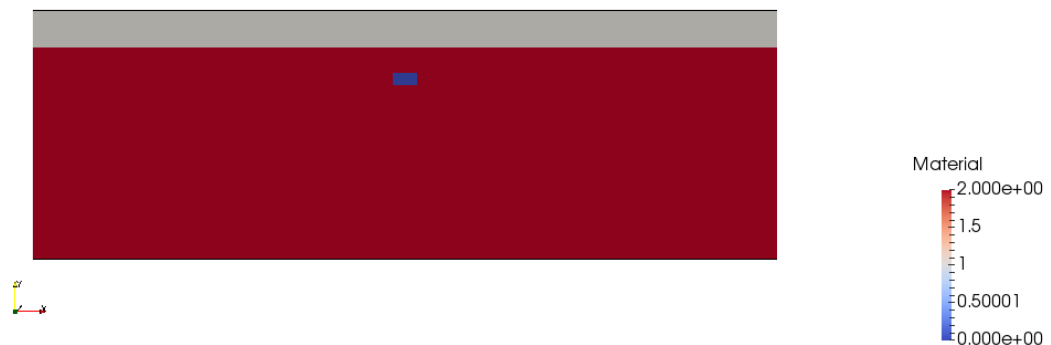
Fig. 3.3: Example Model

3.4. Generation of A-Scan

An A-Scan is a recording of the change in the voltage levels when the signal strikes a target in the domain within the time window. Hence a plot of Voltage strength versus Time i.e Fig 3.4 shows the A-Scan of a metal target being intercepted by the signals transmitted by the transmitting antenna and received by the receiving antenna. When Ez direction is considered, the voltage levels across Ex and Ey will be 0 and thus it can be seen from the A-Scan that the electric fields vary only in Ez-direction. The current being proportional to the electric field also varies only in the Iz-direction and remains zero in the Ix-Iy directions. The magnetic field being perpendicular to the electric field remains zero in the Hz-direction and varies in both Hx and Hy direction. From the graph of Ez versus Time the first variation is when the signal strikes the air-ground interference and the next variation is caused due to the target.
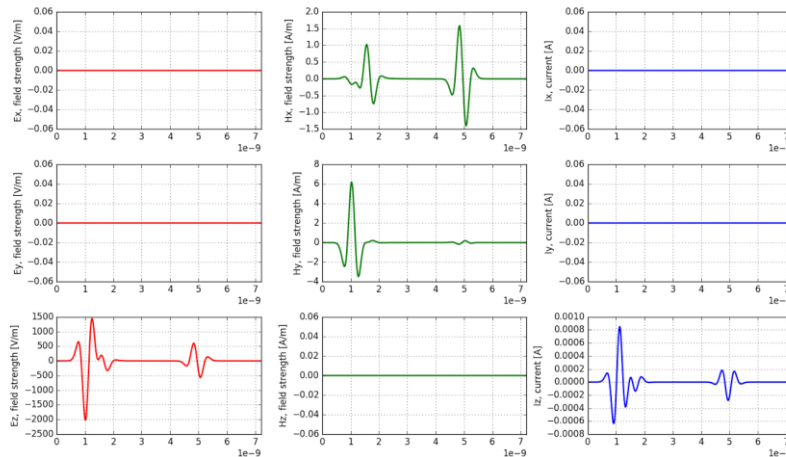
Fig. 3.4 Field outputs from a model of a metal cuboid buried in a dielectric half-space

3.5. Generation of B-Scan

A B-Scan is generated by the column-wise concatenation of A-Scans. For the example model considered, 70 A-scans were taken with a step size of 0.01m. After concatenation we get a matrix where the number of elements in one row equals the number of scans and the number of elements in one column equals the time domain/ time step.
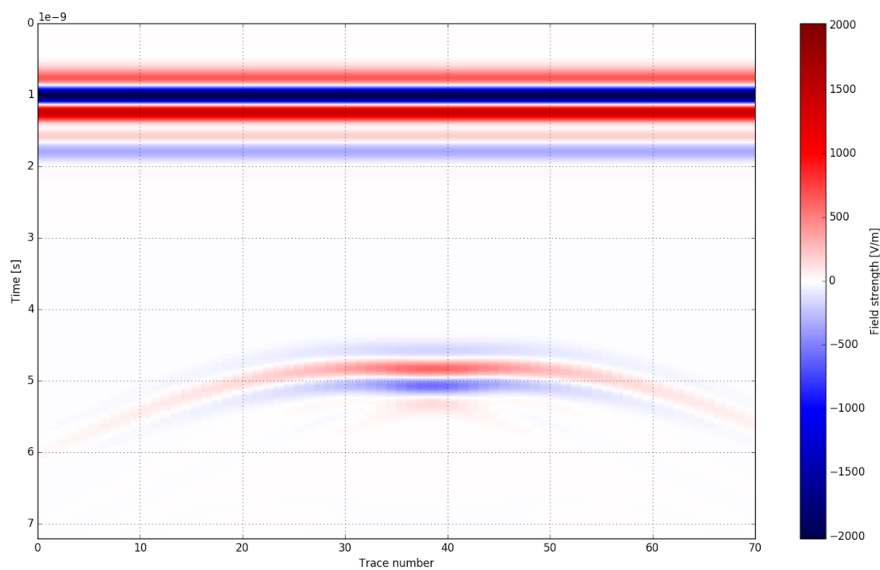
Fig. 3.5: B-scan of model of a metal cuboid buried in a dielectric half-space

Since an image is nothing but a matrix, the voltage levels correspond to the pixel intensity and thus the final output image is as shown in Fig 3.5. In the B-scan the hyperbola corresponds to the target and the top layers of the B-Scan correspond to the air-ground interface and the antenna crosstalk.

3.6. Clutter Classification

Clutter is the major factor that limits the detectability of landmines. Clutter is caused not only by random inhomogeneity in the soil and its topological variations but also by various deterministic reflectors , such as small metal fragments, shrapnel, spent bullet and cartridge cases, puddles of water, tufts of grass, animal burrows, cracks and fissures in the ground, rocks and stones. On the basis of the arrival time of the clutter signal, the clutter can be classified as surface clutter (reflections from the air-ground interface) or subsurface clutter (reflections from all kinds of inhomogeneity in the ground).The global landmine crisis is creating immense social and economic problems worldwide. Safe and cost effective methods for clearing these mines are therefore needed. A promising sensor for detecting anti-personnel mines is ground penetrating radar (GPR). The GPR data, however, is distorted due to very high levels of interfering signals or clutter which leads to an unacceptably large number of false alarms.

In GPR based landmine detection, there are mainly four clutter components, namely,

1. Antenna crosstalk: Antenna Cross-talk is an effect in which signals from one antenna are picked up by an adjacent antenna, causing an erroneous correlation. Antenna cross-talk is a quasi-stationary signal component.

2. Reflection from the air-ground interface: The signal transmitted does not penetrate the ground due air ground dielectric difference.

3. Additive noise: The additive noise may arise due to the interference of electromagnetic devices, mobile phone waves, radio transmission and television antennas, and electromagnetic wave carrying cables.

4. Scattered signal from mine-like objects and ground anomalies: The scattered signal components come from mine-like objects and ground anomalies such as tree roots, stones, air gaps and reflections resulting from scatters within the soil.

Antipersonnel mines are buried at shallow depths. Thus, returns from the mines and that from the rough ground interface overlap in time. It is very difficult to discriminate these coincident responses. Mines are made out of plastic materials and buried in lossy soil. The relative returns from the mines are therefore very low in energy. Commonly used complex natural resonance frequencies are highly damped due to the lack of dielectric contrast between the soil and the mine and are thus not suitable for detection. The GPR also receives returns from other subsurface inhomogeneity, for example rocks, tree roots, or small pieces of metal ground, which leads to high levels of false alarms.

CHAPTER 4

PROPOSED ALGORITHM

PROPOSED ALGORITHM

4.1 Block Diagram
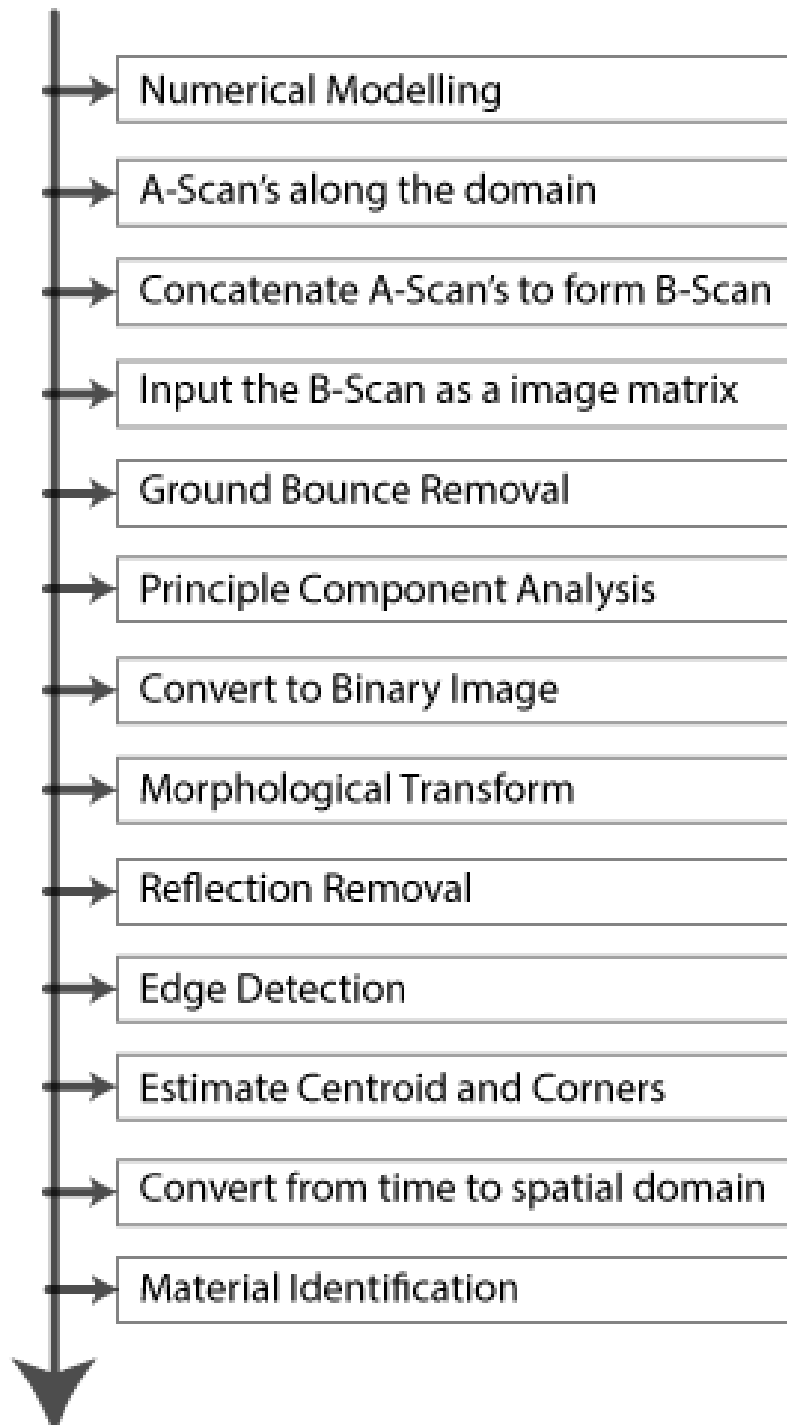
Fig. 4.1: Proposed Block Diagram

4.2 Implementation

4.2.1. Numerical Modeling

The landmine is modeled with appropriate conditions taken into consideration. This has been discussed in detail in chapter 3.3. The modeled scenario is then tested for any irregularities or discrepancies using ParaView software. When the model is verified a scan of the same is taken in parallel.

The parameters considered here are: Domain size- 6x2m, time window- 7.2ns , ricker waveform of amplitude 1 and frequency 1.5GHz, Dipole antennas are placed at a distance of 1.80m from the bottom of the domain, step size - 0.023m and the target landmine which is a perfect electric conductor is placed in the domain with its corners at the points [3.00,1.55], [3.00,1.65], [3.20,1.55] and [3.20,1.65].

The overview of the Numerical model is as shown in Fig.4.2.
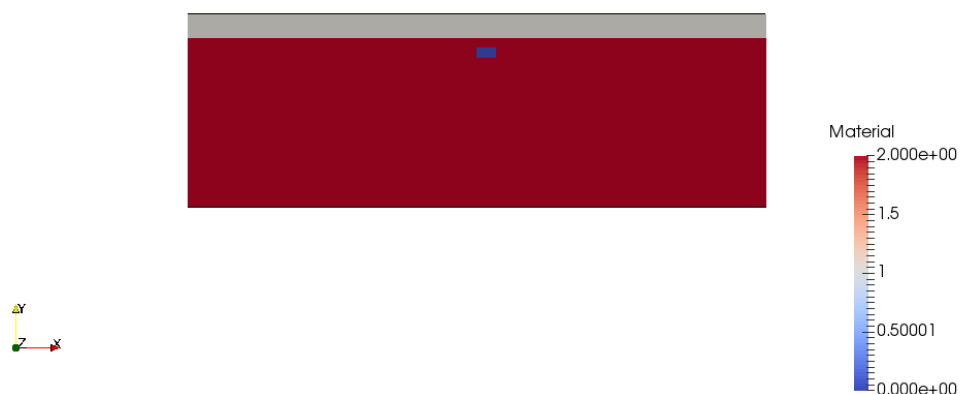
Fig 4.2: Numerical model overview

4.2.2. A-Scan

The generation of A-scan is discussed in detail in chapter 3.4. A single A-Scan is taken right above the target at first to verify whether the target is in the time window or not, if not then numerical modeling is done again. When the A-Scan is generated the values are stored in hdf5 file format and the same is plotted as shown in Fig 4.3. When the scan is taken along Z axis, the variation in voltage

level occurs along Ez axis. Since the Field strength is always perpendicular to the voltage domain, field strength variation occurs along Hx and Hy domain as seen in the graph. The current follows the voltage axis and appears across Iz domain. This can be seen and verified as shown in Fig.4.4.1. The real time simulation is being depicted in Fig.4.3a,b,c.
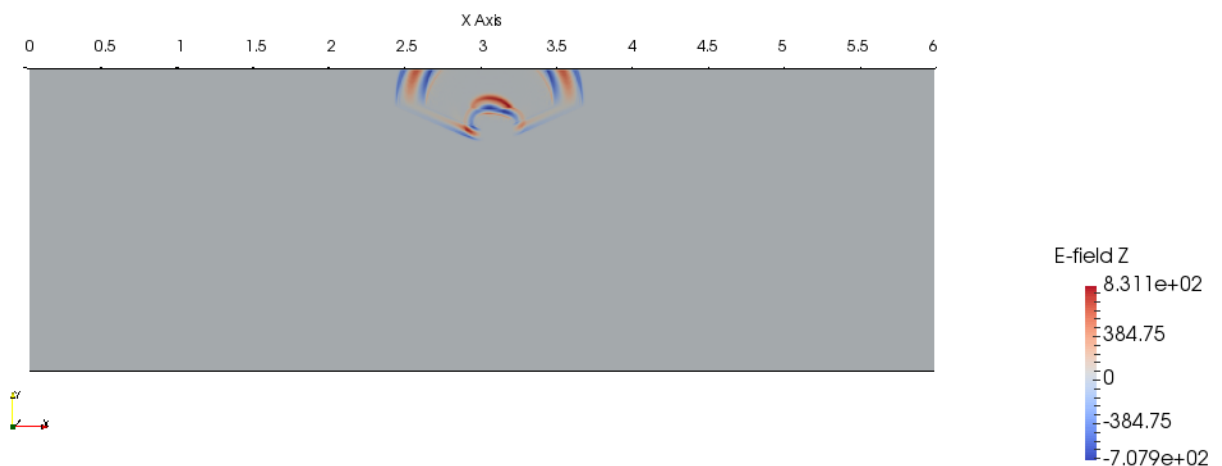
Fig. 4.3a Simulation at 2ns
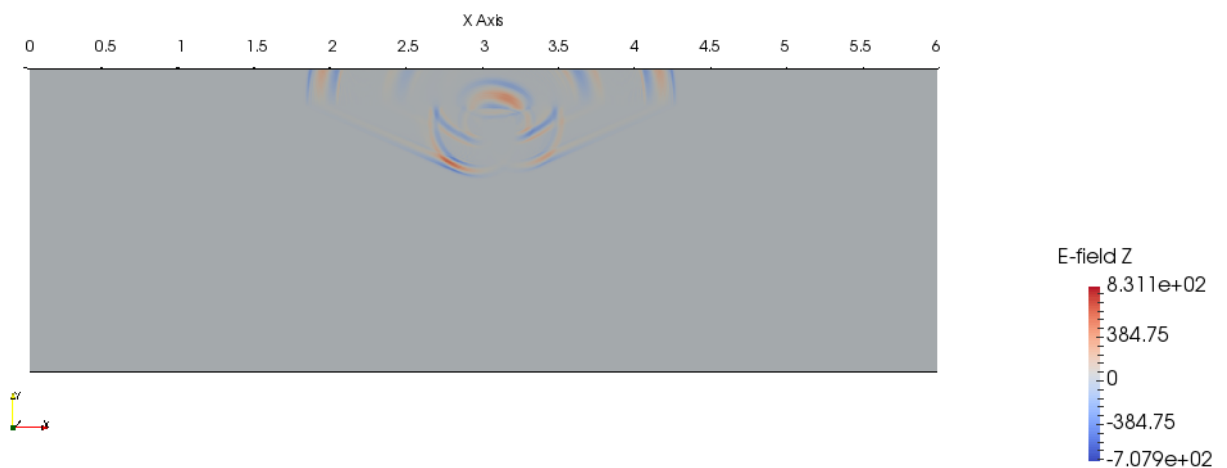
Fig. 4.3b Simulation at 4ns
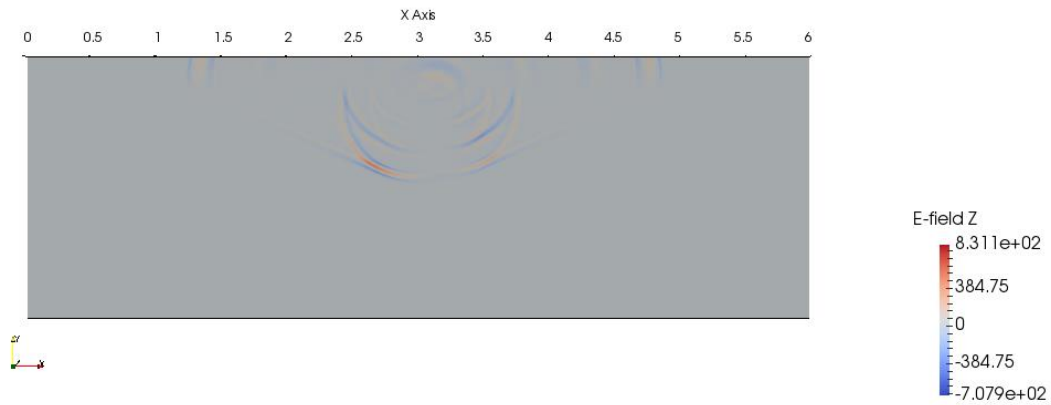
Fig. 4.3c: Simulation at 6ns
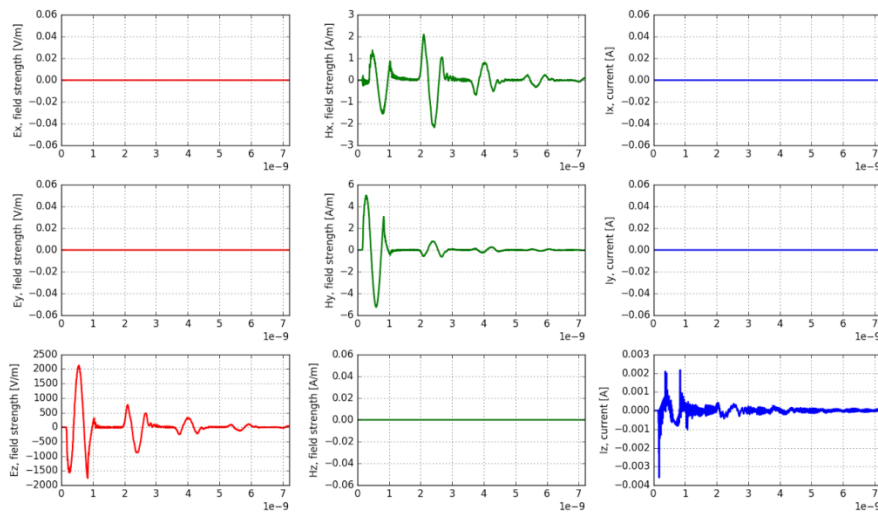
Fig 4.4.1: Field outputs from a model of a metal landmine buried in a dielectric half-space

An A-scan taken at the actual target location is as shown in Fig. 4.4.2. It is evident from the A-scan that the first variation is due to the ground bounce, followed by the actual target and it's corresponding reflections.
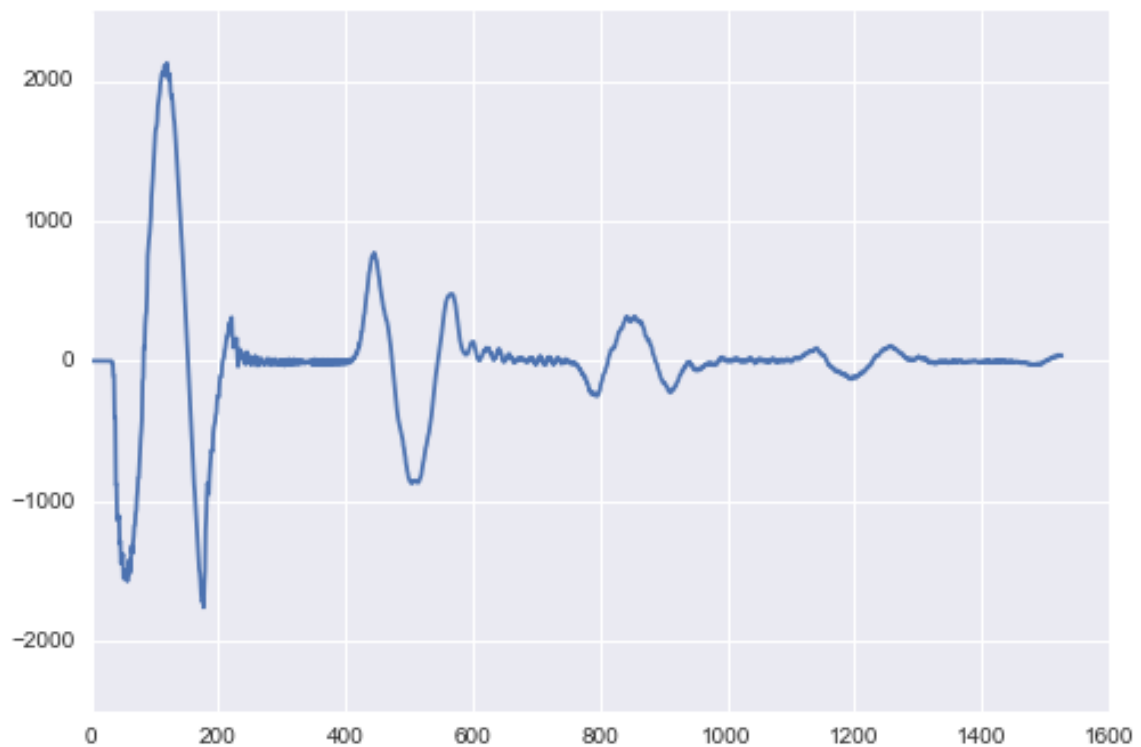
Fig. 4.4.2: A-Scan at actual target location

4.2.3. B-Scan

The generation of B-scan is discussed in detail in chapter 3.5. Since each A-scan now is in hdf5 file format, we need to initialize a numpy.ndarray and concatenate each A-Scan as a single column. Now that we have the final matrix, we can consider this as an image and an image is nothing but a matrix with pixel values. But here, pixel values are the voltage intensity values recorded during computation by GprMax using the FDTD method. Fig 4.5 depicts the B-Scan of that of a metal landmine.
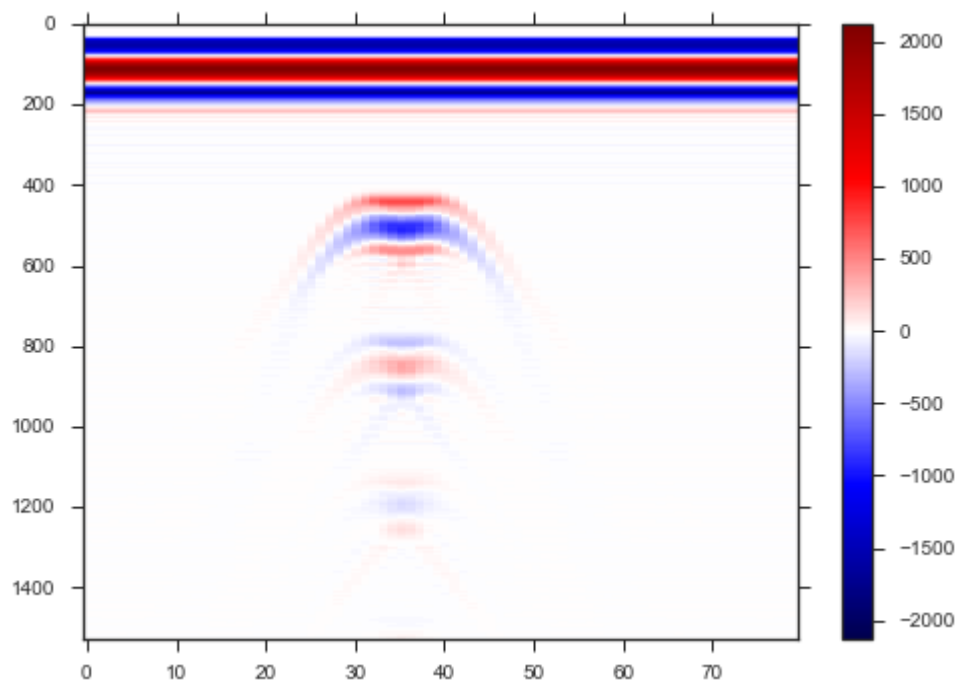
Fig. 4.5: B-scan of model of a metal landmine buried in a dielectric half-space

4.2.4. Ground Bounce and Antenna Crosstalk Removal

The term ground bounce is often used for the effect due to the radar wave being reflected at both the air-ground interface and at the non-ideal antenna. Ground bounce often totally dominates the raw GPR echogram. For the data to be useful for interpretation, the ground bounce must be removed or suppressed by some means. This process is also called "antenna characteristics and air-ground interface de- embedding" or "clutter reduction", both which are more or less equivalent with ground bounce removal.

The algorithm evaluates the intensities of the pixels in the B-scan image. It is an iterative process where all the pixel intensities in each row are being considered at a time. The algorithm zero pads the rows with the same pixel intensities throughout and this happens to be the air bounce clutter in the B-scan. Fig.4.6.1 shows the B-Scan data after the removal of ground bounce and antenna crosstalk. Fig.4.6.2 shows the A-scan data after removal of ground bounce and antenna crosstalk removal.
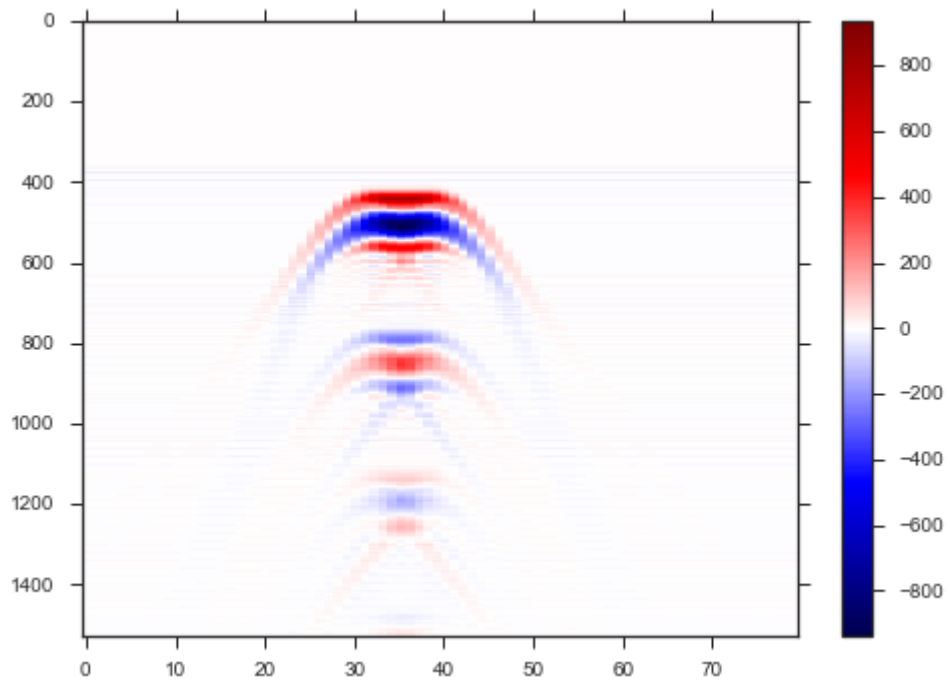
Fig. 4.6.1: B-scan of model of a metal landmine after ground bounce and antenna crosstalk removal
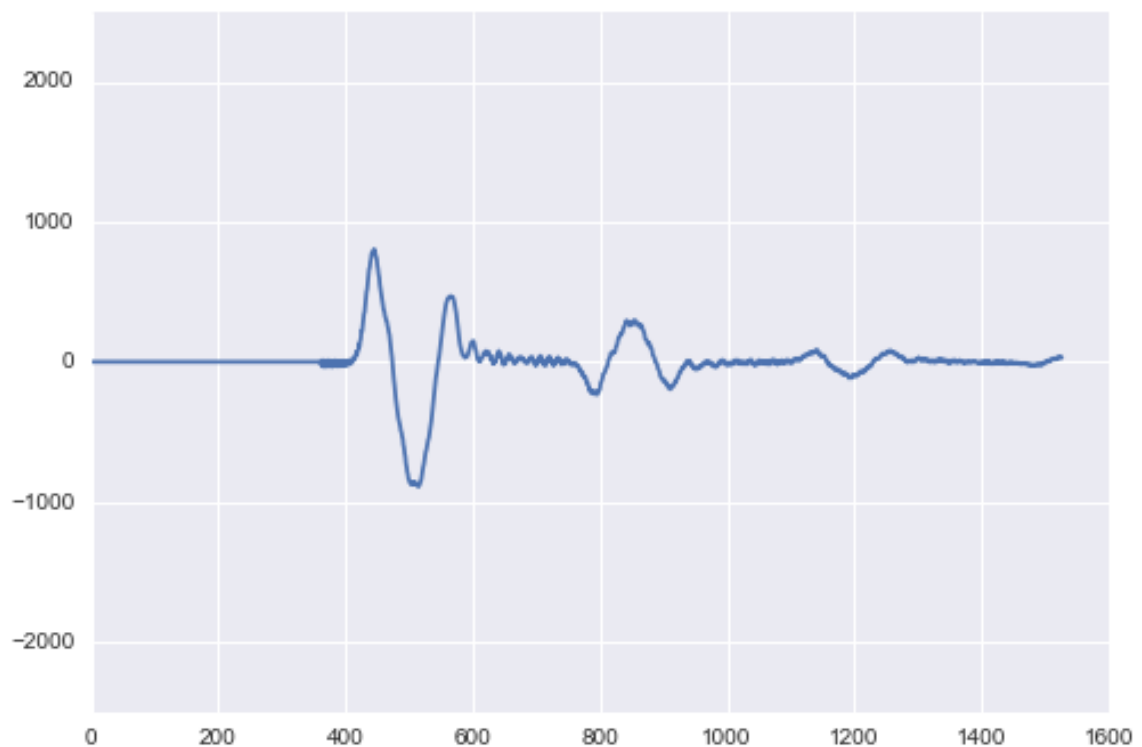
Fig. 4.6.2: A-Scan after ground bounce and antenna crosstalk removal

4.2.5. Principle Component Analysis

Principle Component Analysis is the oldest and the most widely used statistical multivariate technique which finds a pattern in the data under consideration. It can be further extended towards dimensionality reduction by extracting important features which are necessary and ignoring the ones which aren't. It finds its application in face recognition, compression, neuroscience etc.

PCA incorporates a mathematical method called orthogonal transformation to transform a number of possibly correlated variables into a smaller number of linearly uncorrelated variables called principle components. Mathematically, it can be detailed as the orthogonal linear transformation of data onto a new coordinate system such that the greatest variance lies on the first coordinate (called the first principle component), the second greatest variance on the second coordinate, and so on.

A. Principle Component Analysis Algorithm

The algorithm proceeds as follows and is explained for reducing clutter:

1. The antenna crosstalk and ground bounce cleared data is given as input
2. Number of components/Eigenvectors possible for an image of m x n is n.
3. Once Eigenvectors and Eigenvalues are found out, mathematical steps explained below, Eigenvalues are arranged in descending order and so are the corresponding Eigenvectors. Note that the sum of all Eigenvectors is always 1. The Eigenvectors that were found out are plotted in the transformed coordinate system and is as shown in Fig.4.7.
4. More the Eigenvalue more the information content the corresponding Eigenvector will carry and thus selection of Eigenvectors needs to be done appropriately.
5. Thus, arranging it in descending order and summing from the first Eigenvector until 50% of the information content is present. Here, 50% of the information content will be the sum of the Eigenvalues until 0.5. The plot of information content of each Eigenvectors arranged in descending order is as shown in Fig.4.8.

6. Once the number of Eigenvectors who's Eigenvalues adds up to 50% of the content is determined, only those Eigenvectors are considered and the rest is ignored. This is shown in Fig.4.9.

7. The final selected Eigenvectors are now transformed back to the original coordinate system/domain as shown in Fig.4.10.

B. Stepwise Mathematical Execution of the PCA Algorithm

- Let us assume that each row in the input image, represented by T as:

$$T_1, T_2, T_3, \ldots\ldots\ldots\ldots\ldots, T_M$$

- The mean, ψ is obtained by:

$$\psi = \frac{1}{M} \sum_{n=1}^{M} T_M$$

Therefore, each row differs from the *mean* by:

$$\emptyset_n = T_n - \psi$$

- Obtaining the *covariance matrix, C*:

$$C = \frac{1}{M} \sum_{n=1}^{M} \emptyset_n \emptyset_n^T$$

$$= A A^T$$

Where $\emptyset_n^T$ is the transpose of $\emptyset_n$, and *A* is:

$$[\emptyset_1, \emptyset_2, \emptyset_3, \ldots\ldots\ldots\ldots\ldots, \emptyset_M]$$

This covariance matrix consists of large vectors. When PCA is applied to this matrix, a set of *M* orthonormal Eigenvectors is obtained: $\mu_1, \mu_2, \mu_3, \ldots\ldots, \mu_M$. The contributions of individual row of the image T are represented by a Eigenvalue vector ω:

$$[\omega_1, \omega_2, \omega_3, \ldots\ldots\ldots\ldots\ldots, \omega_M]$$

Where ω is:

$$\omega_k = \mu_k^T \cdot \emptyset_k$$
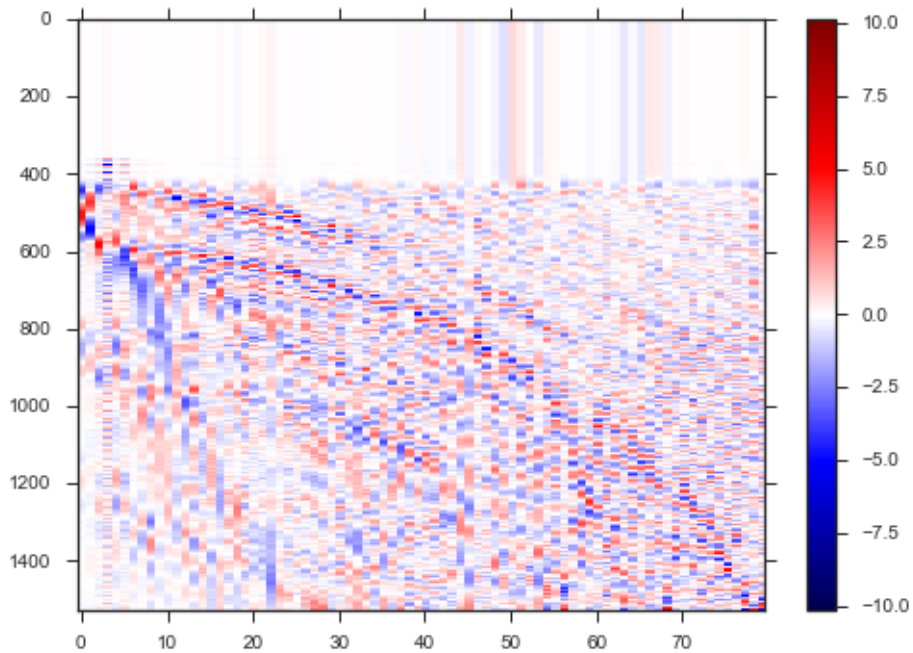
Fig. 4.7: A plot of Eigen Vectors plotted in decreasing order of their Eigen Values
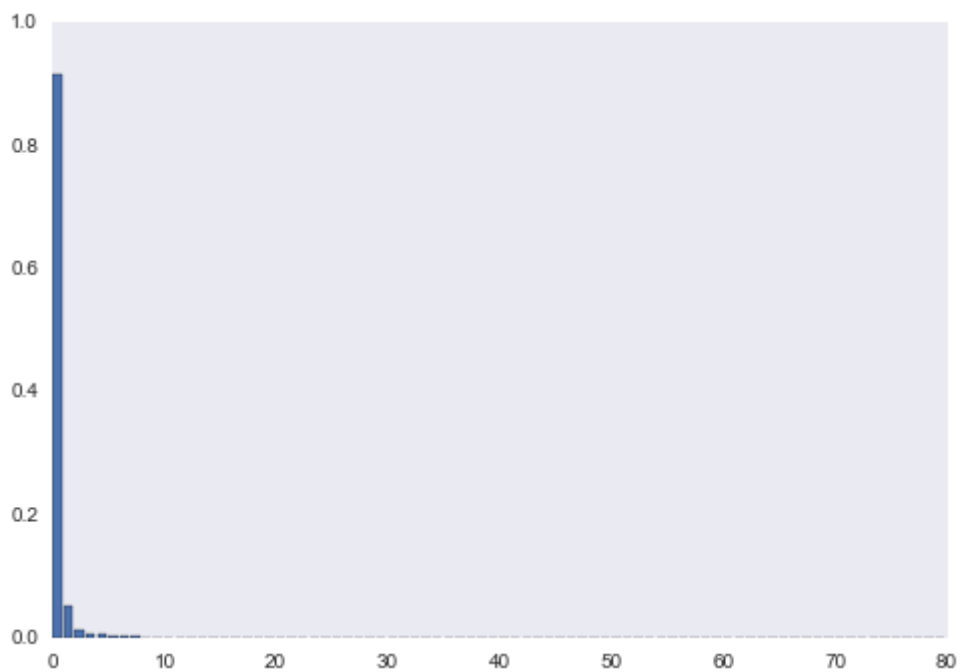
Fig. 4.8: A plot of Eigen Values in decreasing order

In this scenario, since the first Eigenvector only contains 90 percent of the total information content, only it is considered. But in other cases when there are multiple targets then multiple Eigenvectors are being considered.
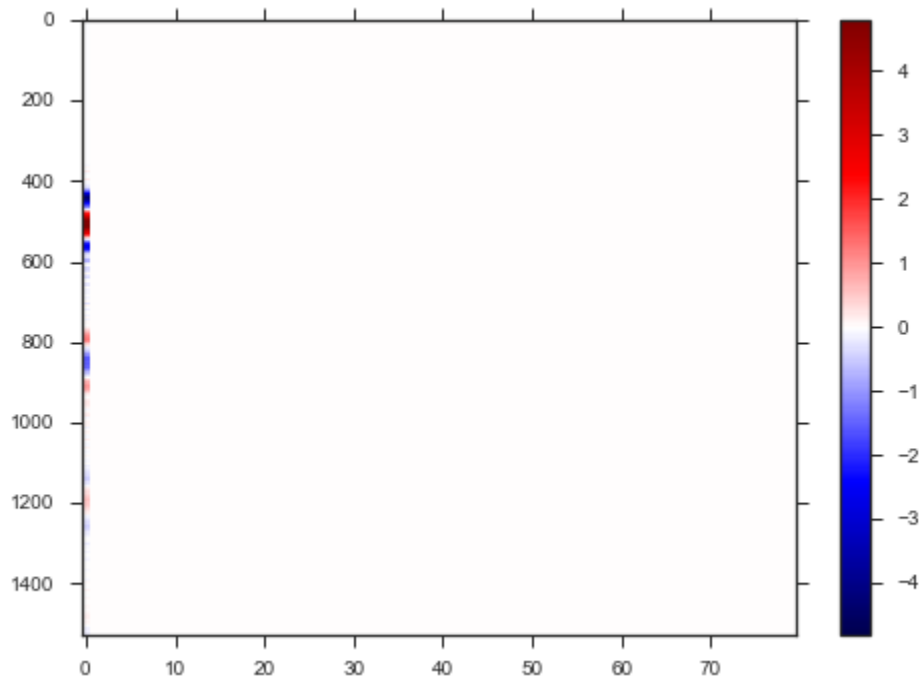
Fig. 4.9: Considered Eigenvectors with 50% information content
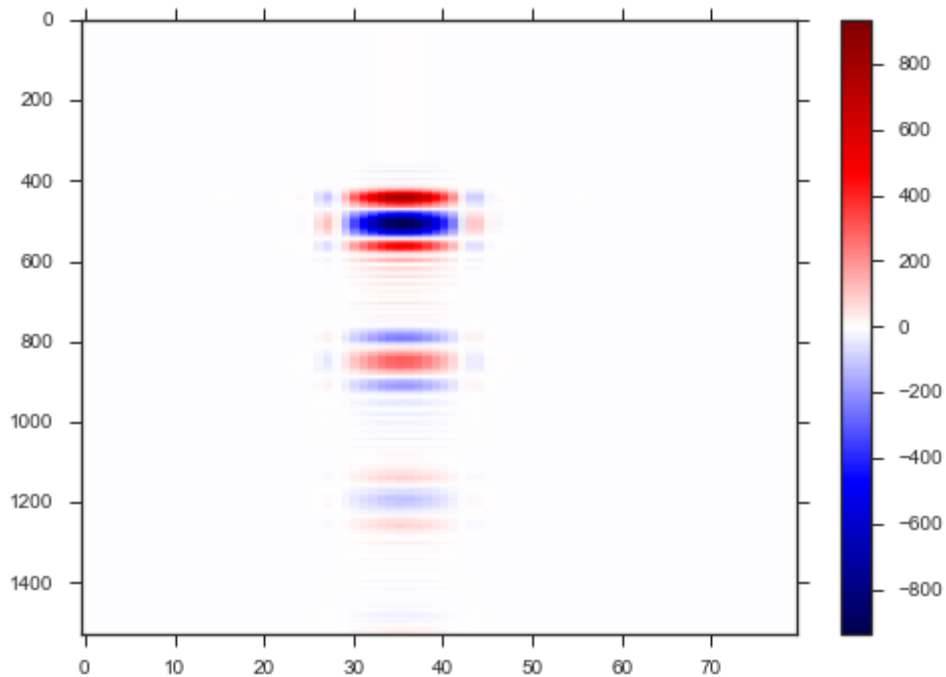
Fig. 4.10: Transformed Eigenvectors to the original domain

4.2.6. Image thresholding and Conversion to binary

As a pre-processing stage before applying morphological transform, the image has to be thresholded and converted to binary. Our point of interest is the blue region where the landmine is located. It will be explained in the result section as to why sine waveform produces negative values in between and positive values in the border. For thresholding, after much trial and error, the pixels who's intensity are greater than -50 are mapped to 0 and those less than -50 are mapped to 1. The resulting image is as shown in Fig.4.11.
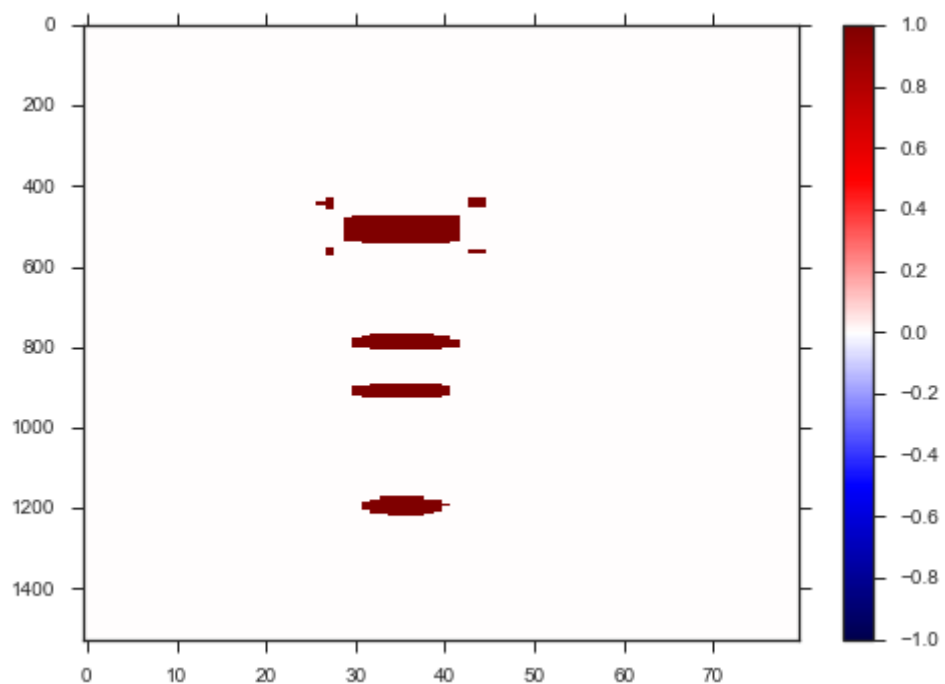
Fig. 4.11: Binary Thresholding

4.2.7. Morphological transform

Morphological transforms are a collection of non-linear operations which involve shape or morphological features in an image. It depends on relative ordering of pixel values and not on the numerical values. As elimination of pixels of non-interest is of priority, Erosion Morphological Transform is put into use here.

In order to eliminate minor clutter data such as reflections from ground anomalies, unwanted minute particles which cause minute changes in the voltage level, Erosion Transform will produce the intended results. The basic effect of the operator on a binary image is to erode away the boundaries of regions of

foreground pixels. The erosion operator takes two pieces of data as inputs. The first is the image which is to be eroded. The second is a (usually small) set of coordinate points known as a structuring element (also known as a kernel). It is this structuring element that determines the precise effect of the erosion on the input image. The structuring element used here is a 5x5 unitary matrix. Thus the foreground pixels are represented by 1's and background pixels by 0's. Thus only the groups of pixels in the image that match with the structuring element are retained and the other boundary regions are being eroded as shown in Fig.4.12.
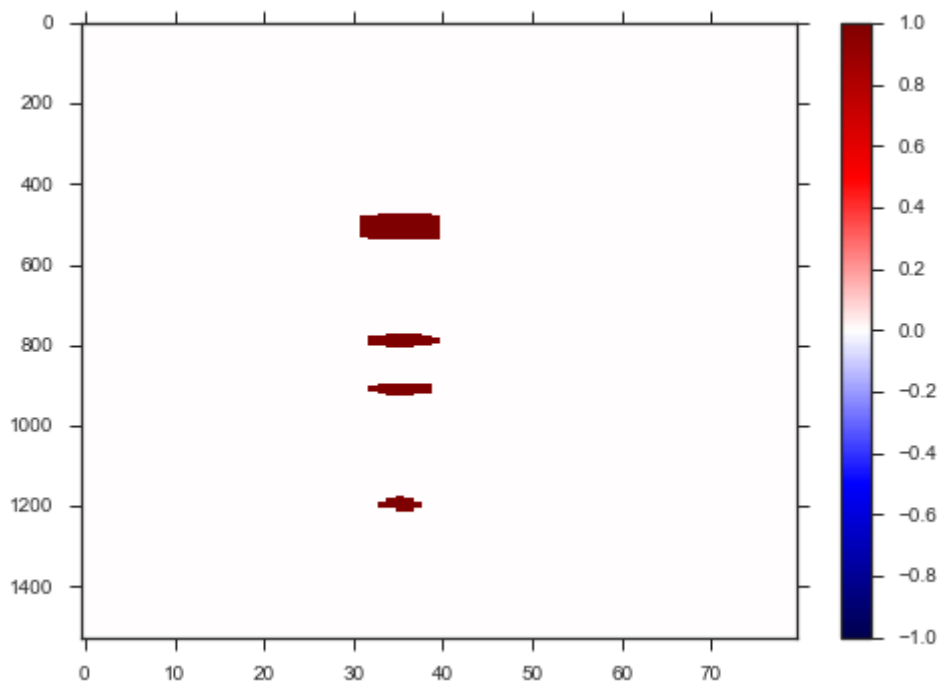
Fig. 4.12: Morphologically Transformed B-scan

4.2.8. Reflections from the target

The reflections are due to dimensionality of the landmine. As and when the electromagnetic wave encounters a landmine surface it gets reflected back and the same can be interpreted in the B-scan. The reflections also vary according to the material of the landmine to be detected. Like for example, B-scan of metal landmines tend to have more than two reflections and that of plastic landmines will have only one reflection.

The reflections are removed by considering all the pixel values of the B-scan image column-wise. In each column the largest continuous set of ones are retained and the corresponding pixel values are made zero. Thus all the pixels

below the actual target which would correspond for the reflections are being removed.

For example, if a column reads,

0,0,0,0,0,0,1,1,1,1,1,0,0,0,0,0,0,0,1,1,1,0,0,0,1,1,0,0,0,0,0,1,0,0,0,0

Then the resultant will be,

0,0,0,0,0,0,1,1,1,1,1,0,0,0,0,0,0,0,0,0,0,0,0,0,0,0,0,0,0,0,0,0,0,0,0,0

This method will work for all scenarios as:

- Reflections always appear below the actual target

- The intensity of the reflections keeps on decreasing.

- Thus, the group of ones will be highest for the target and less for the reflections.

- This will also remove smaller intensities caused by anomalies and minute grains of the soil.

But, if one landmine is kept right below another landmine, then the bigger dimension landmine will be considered and the smaller landmine will be removed by this method. But in real world scenario such conditions are not seen or rather rare. This method is employed and done for the columns, and the result is as seen in Fig.4.13.1. Fig. 4.13.2 shows the A-scan data after removal of reflections.
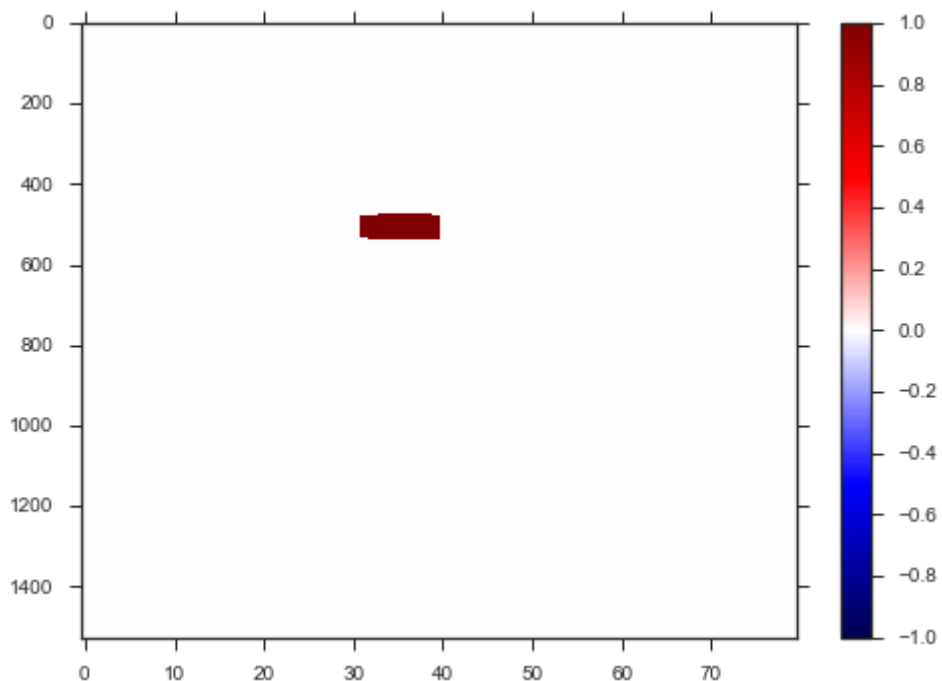
Fig. 4.13.1: B-Scan data after removal of reflections
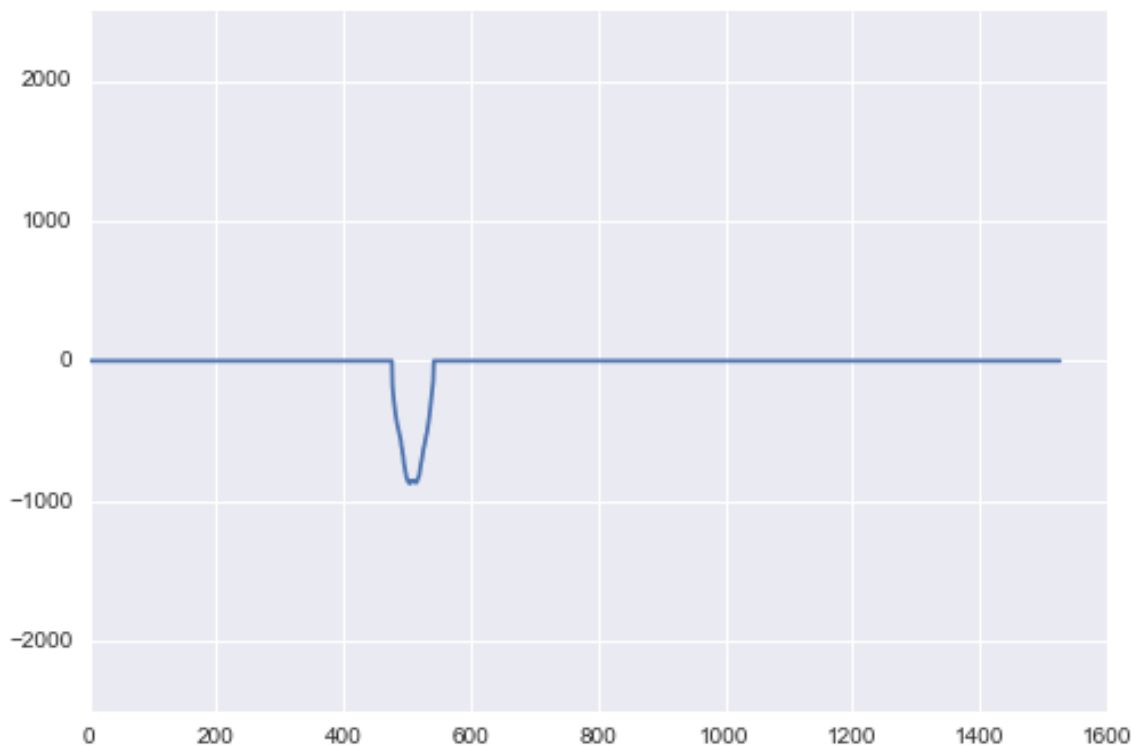
Fig. 4.13.2: A-scan after removal of reflections

4.2.9. Estimating the Position of Landmine

The border following algorithm proposed in the paper "Topological Structural Analysis of Digitized Binary Images by Border Following" [9] is been implemented here.

Border following is one of the fundamental techniques in the processing of digitized binary images. It derives a sequence of the coordinates or the chain codes from the border between a connected component of 1-pixels (1-component) and a connected component of 0-pixels (background or hole). Thus for the image shown in Fig 4.13 by implying border following algorithm, the sequence of 1- component is found out and a rectangle or a bounding box is estimated from that sequence. This is done so by considering the largest possible connection that is possible between each 1- component. Once the rectangle is estimated, the coordinates of the corners are outputted. By using Euclidean distance the dimension of the landmine can be found out and by using mid-point formula the centroid of the target can be estimated. The estimated target locations are as follows:

Parameter	Co-ordinates [x,y]	
Centroid	(35,509)	
Corners	[31, 541]	[31, 477]
	[39, 477]	[39, 541]

4.2.10. Convert from time to spatial domain

Speed is equal to distance/ time and the same concept can be expanded here as speed of signal is equal to wavelength * frequency. Since we know the frequency of the signal and the permittivity of the medium we can compute the speed of the signal by c/sqrt (permittivity). Substituting the same we can compute the wavelength. Once we have the wavelength we can multiply it with the time to get the actual depth of the mine. The target locations after conversion are as follows:

Parameter	Co-ordinates [x,y]	
Centroid	(3.125, 1.5959815429637292)	
Corners	[3.033,1.58687548]	[3.033,1.6050876]
	[3.217,1.6050876]	[3.217,1.58687548]

4.2.11. Material Identification

The material identifications are done prior to the reflection removal part of the algorithm. By evaluating the number of groups of ones in the columns of the image, the number of reflections of that landmine can be estimated. Thus by keeping the number of reflections as reference the type of material of the landmine can be found out and recorded.

4.2 Drawbacks of the algorithm

1. If a landmine is placed just below another landmine then the algorithm would fail to detect both the landmines. The landmine closer to the ground would be detected and one underneath would go undetected. This is because of the column-wise pixel evaluation and a valid landmine would be discarded as reflection in the B-scan data. But in reality such cases are very rare.

2. The algorithm tends to output a slight error while determining the landmine location. This is due to image processing operations and such errors are unavoidable.

CHAPTER 5

SIMULATED RESULTS

SIMULATED RESULTS

Different materials of landmines and different types of possible clutter elements are considered in the following test cases. Four different cases of single and multiple targets are considered and in each case externally added Gaussian noise is considered as one of the clutter elements. Water puddles, granites and small stone particles are modeled in the B-Scans and the results in each case are tabulated as shown.

5.1 Single Target: Metal Landmine with Externally Added Gaussian Noise
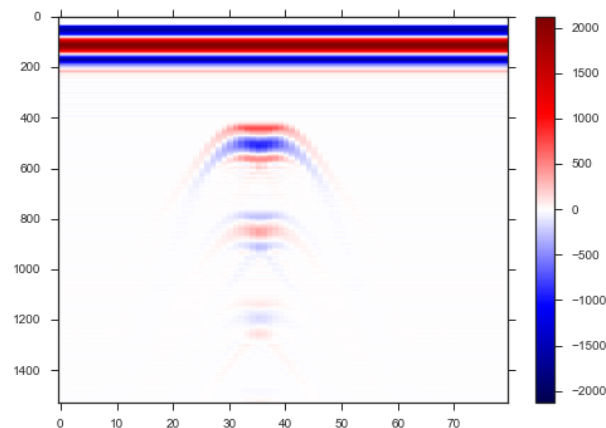
a
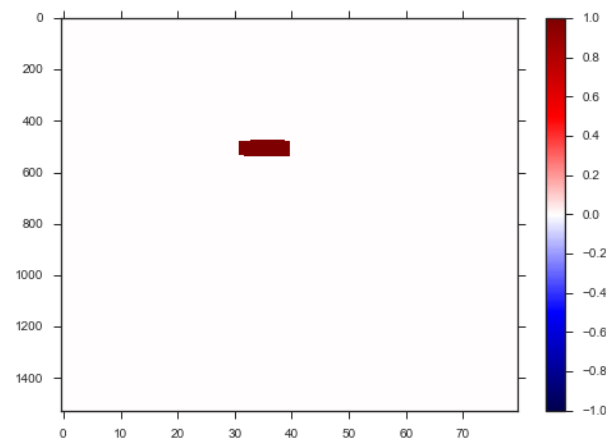
b

Fig.5.1 Generated B-scan and final result obtained using the algorithm

The B-scan of a single metal target is as shown in Fig. 5.1a. The numerical model overview and the real time simulations are shown in Fig. 4.2 and Fig. 4.3 respectively. The working of the algorithm to obtain the final landmine detected image as shown in Fig. 5.1b is explained in the previous chapter. The stepwise explanation of the algorithm is done in the previous chapter and the results for the same are tabulated.

5.2 Two Targets: Metal and Plastic Landmines with Externally Added Gaussian Noise

The numerical modeling and real time simulation when both metal and plastic landmines lie in the same domain are as shown in Fig5.1 and Fig5.2 respectively.
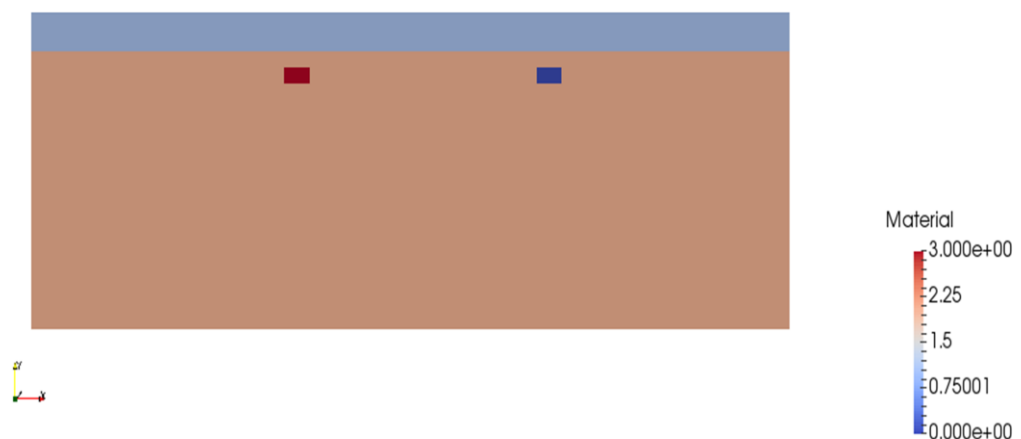
Fig.5.2: Numerical model overview of metal and plastic landmines
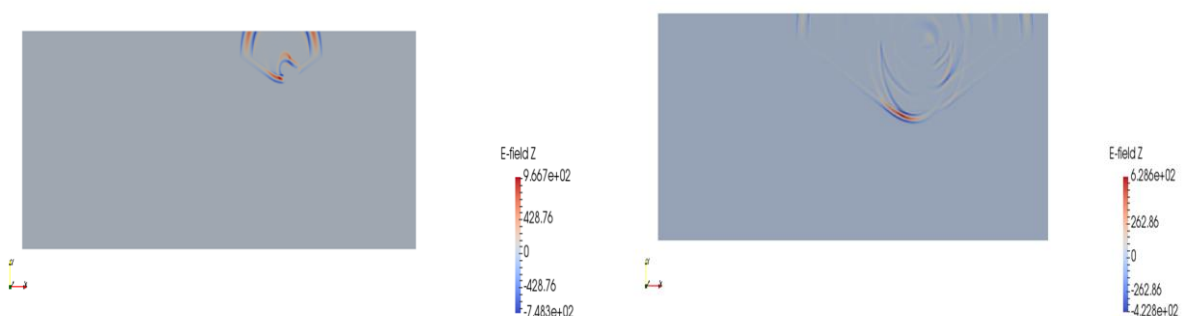
Fig.5.3: Real Time Simulation at 2ns and 6ns

2. Time window – 7.2ns

3. Plastic Landmine Properties and Position:

   Permittivity – 3.3, Conductivity – 1.34

   Permeability – 1, Magnetic Loss – 0

   Position Coordinates: [2.00,1.5], [2.00,1.6], [2.20,1.5], [2.20,1.6]

4. Metal Position:

   Position Coordinates: [4.20,1.5], [4.20,1.6], [4.40,1.5], [4.40,1.6]

When the algorithm is applied:
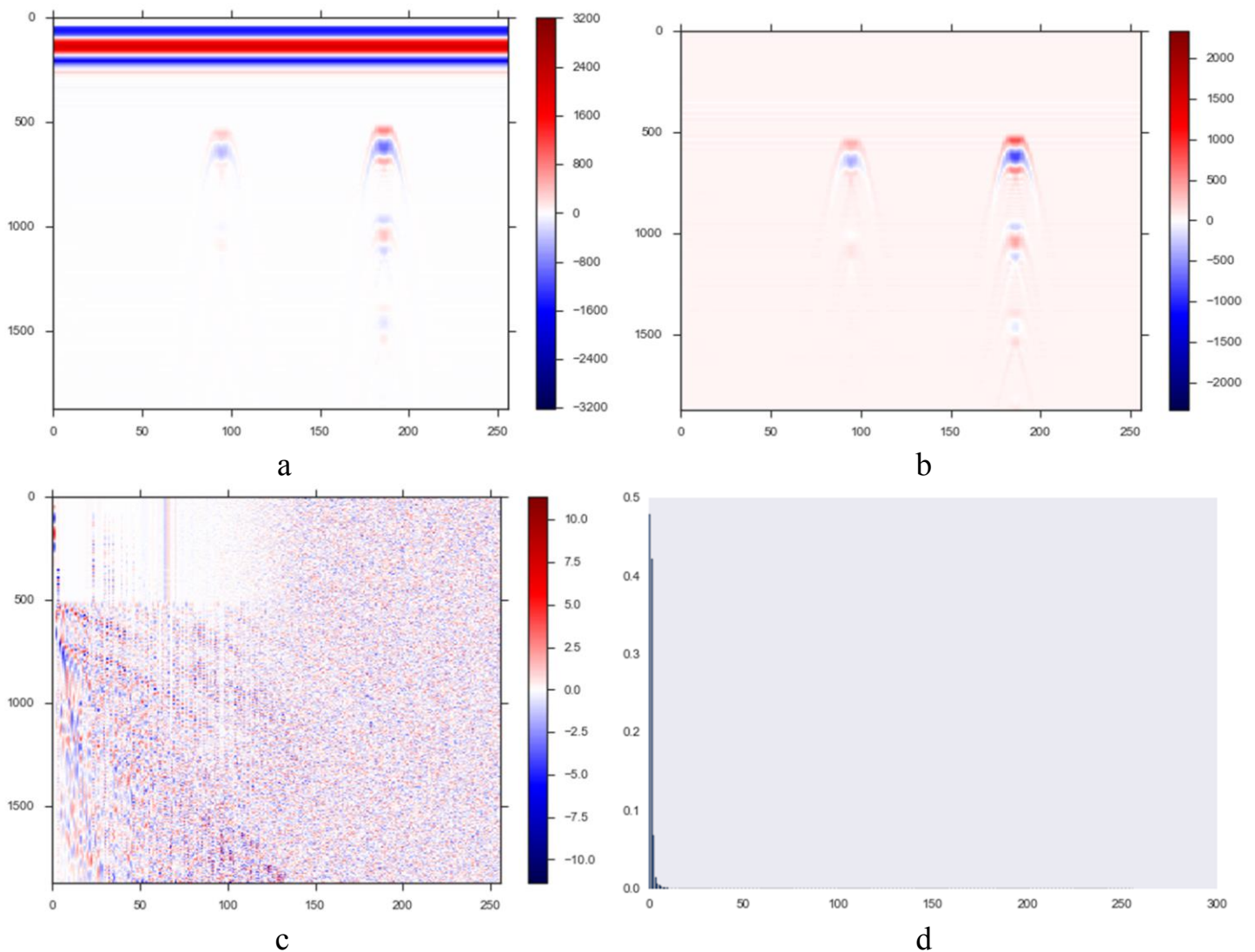
Fig. 5.4: Ground Bounce Removal and Eigenvectors Consideration
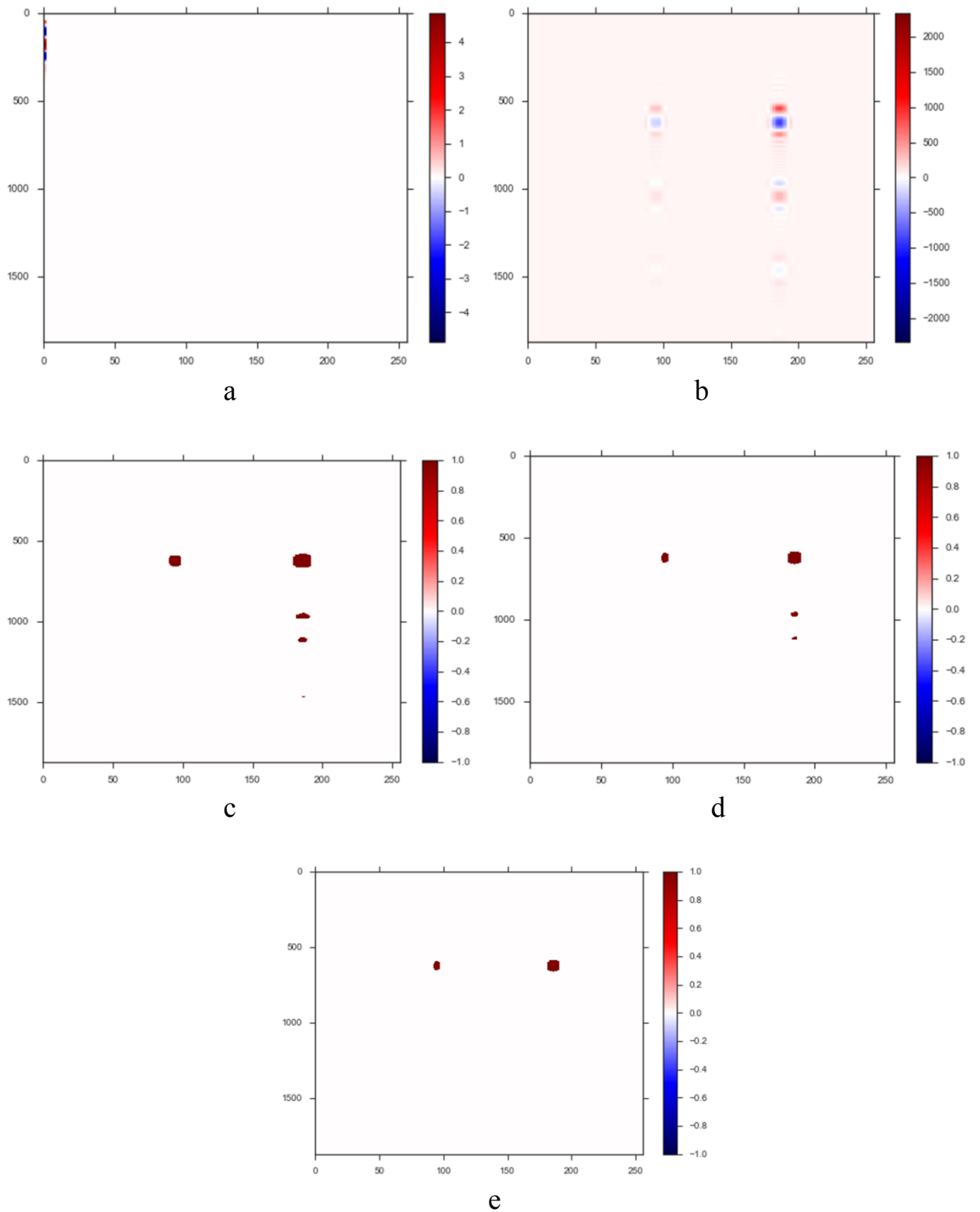
Fig. 5.5: Reflection Removal and Targets Location Estimation

Fig.5.4a depicts the B-scan data containing plastic and metal landmines. Plastic landmine is the first landmine encountered and metal landmine being the second. Fig.5.4b shows the B-scan data after removal of antenna crosstalk and ground bounce. Fig 5.4c and Fig 5.4d depicts the Eigen vectors of the entire B-scan data and the information content in each of these Eigen vectors respectively. The principle component analysis is applied to remove as much unwanted information as possible. In this case, the first Eigen vector contains almost 50 percent of the information content and thus only this vector is considered. Fig.5.5a shows the selection of the first Eigen vector and Fig.5.5b shows the B-scan data obtained by multiplying the selected Eigen vector with the entire B-scan image. Fig 5.5c and Fig.5.5d show the binary transformed and morphologically transformed image respectively. After removing the reflections, only the areas of interest remain which depict the landmines and are represented in Fig.5.5e. Edge detection and co-ordinates estimation is being done and tabulated as shown.

Results Obtained using the Algorithm:

First detected landmine (plastic):

Parameter	Co-ordinates [x,y]	
Centroid	[94,626]	
Corners	[92,656]	[92,595]
	[96,595]	[96,656]

Second detected landmine (metal):

Parameter	Co-ordinates [x,y]	
Centroid	[185,625]	
Corners	[181,664]	[181,587]
	[189,587]	[189,664]

The results obtained are in the time domain. In-order to get the exact estimates of the position and dimensions of the landmine the obtained co-ordinates must be shifted from time domain to the spatial domain. The material of the landmine is decided by estimating the number of reflections.

Results after conversion from time to spatial domain:

Actual location of the first landmine (plastic):

Parameter	Co-ordinates [x,y]	
Centroid	[2.1869, 1.5249]	
Corners	[2.141,1.5179]	[2.141,1.5321]
	[2.233,1.5321]	[2.233,1.5179]

Actual location of the second landmine (metal):

Parameter	Co-ordinates [x,y]	
Centroid	[4.2800,1.5251]	
Corners	[4.188,1.5161]	[4.188,1.5340]
	[4.372,1.5340]	[4.372,1.5161]

5.3 Two Targets and A False Target: Metal and Plastic Landmines with Water Puddle and externally added Gaussian Noise

The numerical modeling and real time simulation when both metal and plastic landmines lie in the same domain along with water puddle and external Gaussian noise are as shown in Fig5.5 and Fig5.6 respectively.
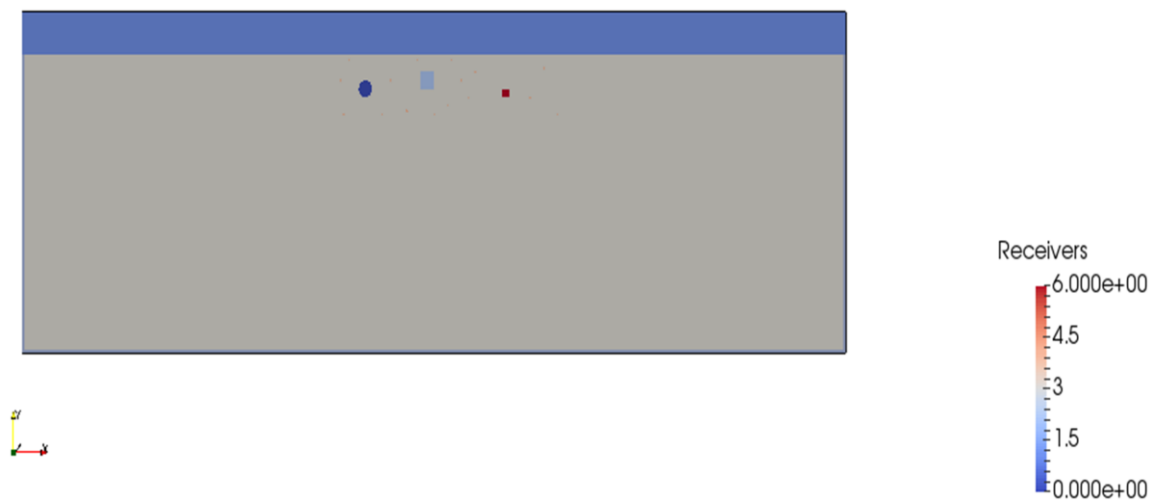
Fig.5.6: Numerical model overview of metal and plastic landmines with water puddle
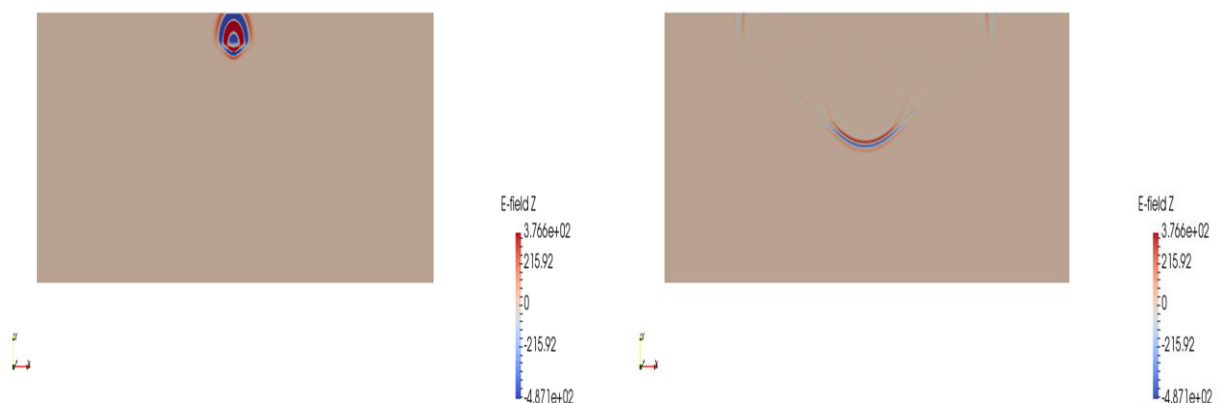
Fig.5.7: Real Time Simulation at 2ns and 6ns

The different parameters considered while modeling are as follows:

1. Domain size – 6x2m
2. Time window – 7.2ns
3. Plastic Landmine Properties and Position:

Permittivity – 3.3, Conductivity – 1.34

Permeability – 1, Magnetic Loss – 0

Position Coordinates: [2.90,1.55], [2.90,1.65], [3.00,1.55], [3.00,1.65]

4. Metal Landmine is a sphere with:

Centre: [2.5,1.55]

Radius: 0.01m

5. Water puddle properties and position:

Permittivity – 4.9, Conductivity – 0.001

Permeability – 1, Magnetic Loss – 0

Position Coordinates: [3.5,1.50], [3.5,1.55], [3.55,1.50], [3.55,1.55]

When the algorithm is applied:

a

b

c

d
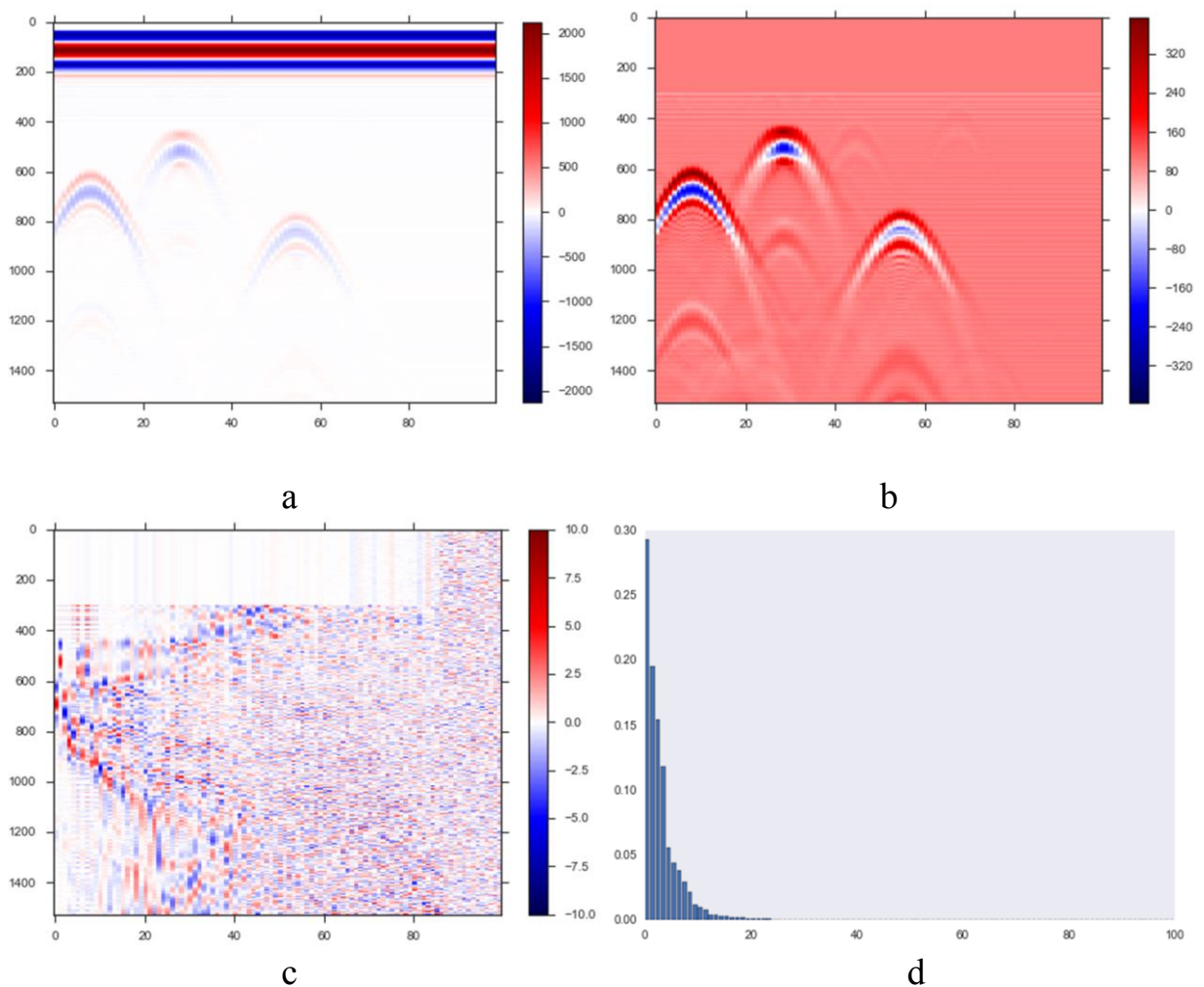
Fig. 5.8: Ground Bounce Removal and Eigenvectors Consideration
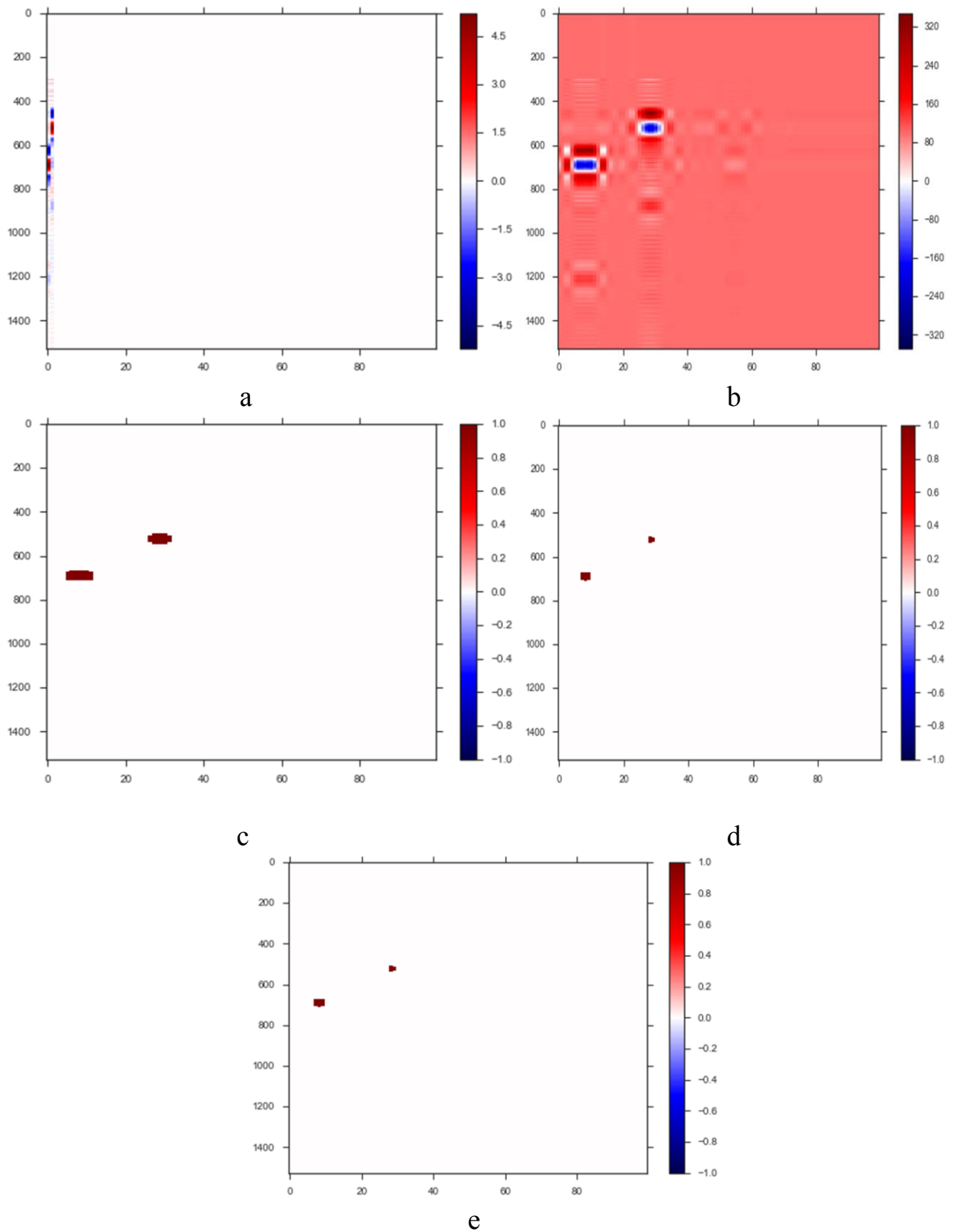
Fig. 5.9: Reflection Removal and Targets Location Estimation

Fig.5.8a depicts the B-scan data containing plastic and metal landmines along with water puddle. Metal landmine is the first landmine encountered with plastic landmine being the second and followed by water puddle. Fig.5.8b shows the B-scan data after removal of antenna crosstalk and ground bounce. Fig 5.8c and Fig 5.8d the Eigen vectors of the entire B-scan data and the information content in each of these Eigen vectors respectively. The principle component analysis is applied to remove as much unwanted information as possible. In this case, the first two Eigen vectors contain more than 50 percent of the information content when considered together and thus only these two vectors are considered. Fig.5.9a shows the selection of the first two Eigen vectors and Fig.5.9b shows the B-scan data obtained by multiplying these selected Eigen vectors with the entire B-scan image. Fig 5.9c and Fig.5.9d show the binary transformed and morphologically transformed image respectively. After removing the reflections, only the areas of interest remain which depict the landmines and are represented in Fig.5.9e. It can be seen from this image that the water puddle is not been considered as a target even though it appears to be one and is eliminated by the algorithm. The two targets of interest are being retained and furthermore edge detection and co-ordinates estimation are being done and tabulated as shown.

Results Obtained using the Algorithm:

First detected landmine (metal):

Parameter	Co-ordinates [x,y]	
Centroid	[8,692]	
Corners	[7,713]	[7,672]
	[9,672]	[9,713]

Second detected landmine (plastic):

Parameter	Co-ordinates [x,y]	
Centroid	[28,526]	
Corners	[28,539]	[28,513]
	[29,513]	[29,539]

Results after conversion from time to spatial domain:

Actual location of the first landmine (metal):

Parameter	Co-ordinates [x,y]	
Centroid	[2.5090,1.4734]	
Corners	[2.486,1.4675]	[2.486,1.4791]
	[2.532,1.4791]	[2.532,1.4675]

Actual location of the second landmine (plastic):

Parameter	Co-ordinates [x,y]	
Centroid	[2.9690,1.5207]	
Corners	[2.969,1.5170]	[2.969,1.5244]
	[2.992,1.5244]	[2.992,1.5170]

5.4 Three Targets and Two False Targets: Two metal and a Plastic Landmine with Granite, Water Puddle and Externally added Gaussian Noise

The numerical modeling of both metal and plastic landmines lying in the same domain along with water puddle, granite and external Gaussian noise is as shown in Fig5.10.
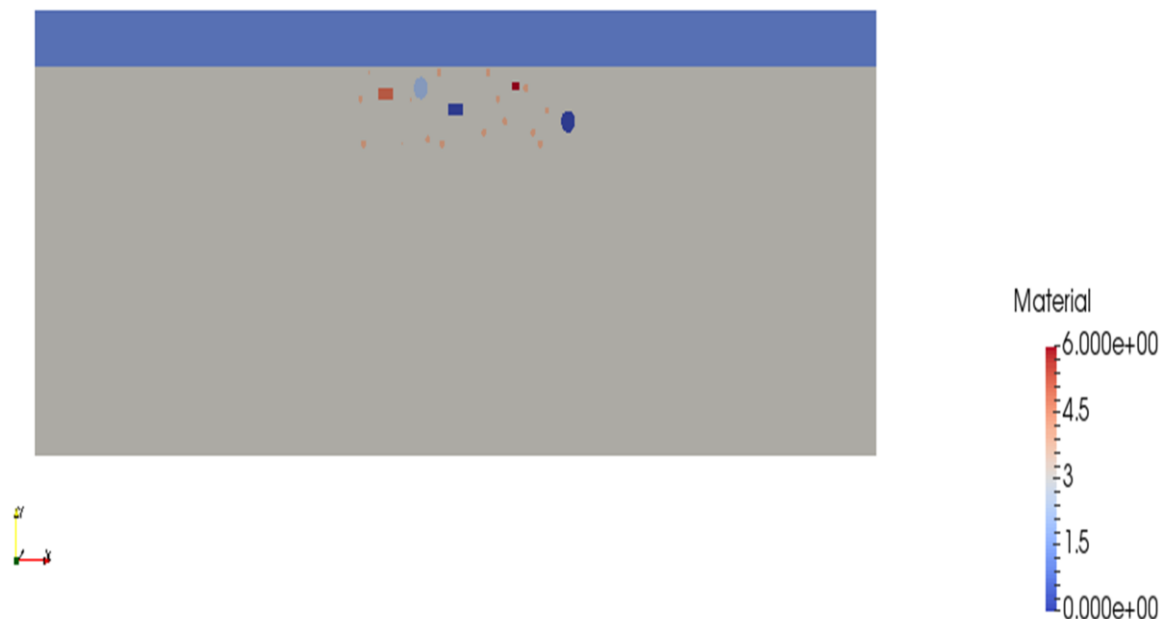
Fig.5.10: Numerical model overview of metal and plastic landmines with water puddle and granite

The different parameters considered while modeling are as follows:

1. Domain size – 6x2m
2. Time window – 7.2ns
3. Plastic Landmine with properties and position:

    Permittivity – 3.3, Conductivity – 1.34

    Permeability – 1, Magnetic Loss – 0

    Position Coordinates: [2.45,1.60], [2.45,1.65], [2.55,1.60], [2.55,1.65]

4. Metal Landmines(sphere and rectangle] with positions:

    Sphere - Centre: [3.8,1.50], Radius: 0.01m

Rectangle - Coordinates: [2.95,1.53], [2.95,1.58], [3.05,1.53], [3.05,1.58]

5. Water puddle is a sphere with properties and position:

Permittivity – 4.9, Conductivity – 0.001

Permeability – 1, Magnetic Loss – 0

Centre – [2.75,1.65], Radius – 0.01m

6. Granite properties and position:

Permittivity – 9, Conductivity – 0.001

Permeability – 1, Magnetic Loss – 0

Position Coordinates: [3.40,1.64], [3.40,1.68], [3.45,1.64], [3.45,1.68]

When the algorithm is applied:

a

b

c

d
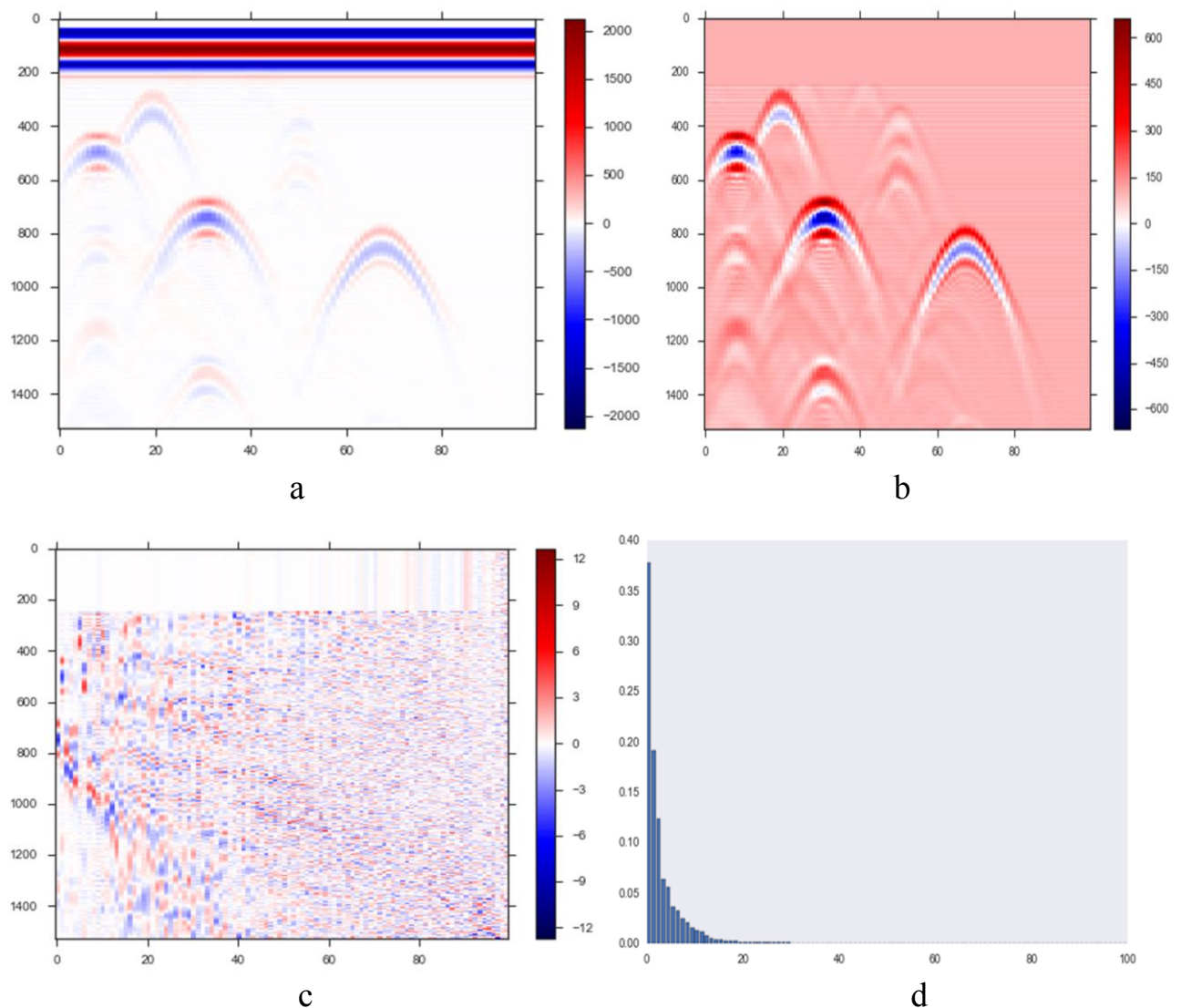
Fig. 5.11: Ground Bounce Removal and Eigenvectors Consideration

a

b

c

d

e
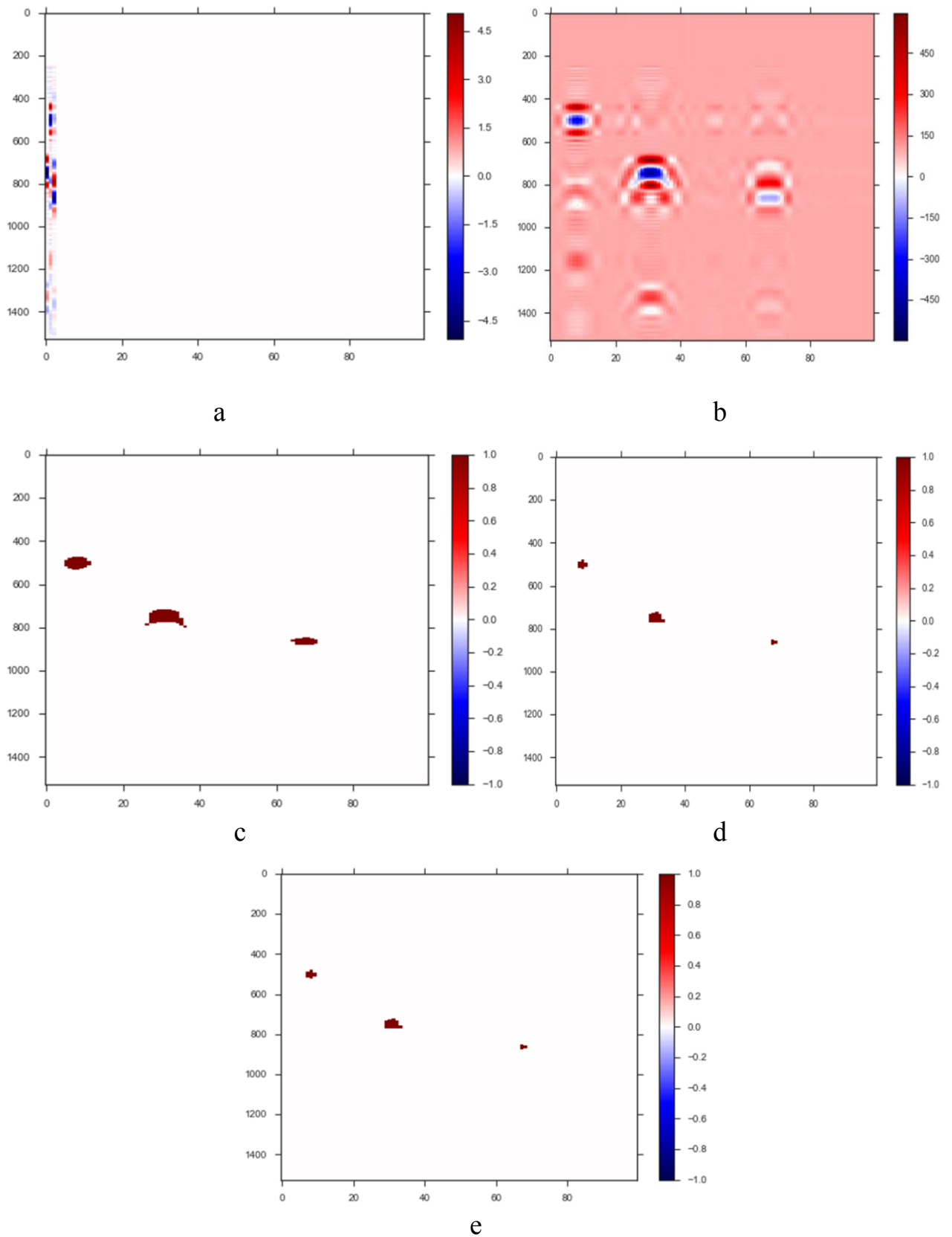
Fig. 5.12: Reflection Removal and Targets Location Estimation

Fig.5.11a depicts the B-scan data containing plastic and metal landmines along with water puddle and granite. Plastic landmine is the first encountered with water puddle being the second followed by metal landmine(rectangle), granite and another metal landmine(sphere). Fig.5.11b shows the B-scan data after removal of antenna crosstalk and ground bounce. Fig 5.11c and Fig 5.11d the Eigen vectors of the entire B-scan data and the information content in each of these Eigen vectors respectively. The principle component analysis is applied to remove as much unwanted information as possible. In this case, the first two Eigen vectors contain more than 50 percent of the information content when considered together and thus only these two vectors are considered. Fig.5.12a shows the selection of the first two Eigen vectors and Fig.5.12b shows the B-scan data obtained by multiplying these selected Eigen vectors with the entire B-scan image. Fig 5.11c and Fig.5.11d show the binary transformed and morphologically transformed image respectively. After removing the reflections, only the areas of interest remain which depict the landmines are represented in Fig.5.11e. It can be seen from this image that the water puddle and granite are not been considered as targets even though they appear to be one and are eliminated by the algorithm. The three targets of interest are being retained and furthermore edge detection and co-ordinates estimation are being done and tabulated as shown.

Results Obtained using the Algorithm:

First detected landmine (plastic):

Parameter	Co-ordinates [x,y]	
Centroid	[7,505]	
Corners	[7,525]	[7,482]
	[9,482]	[9,525]

Second detected landmine (metal rectangle):

Parameter	Co-ordinates [x,y]	
Centroid	[30,753]	
Corners	[29,774]	[29,725]
	[33,725]	[33,774]

Third detected landmine (metal sphere):

Parameter	Co-ordinates [x,y]	
Centroid	[67,864]	
Corners	[66,878]	[66,853]
	[68,853]	[68,878]

Results after conversion from time to spatial domain:

Actual location of the first landmine (plastic):

Parameter	Co-ordinates [x,y]	
Centroid	[2.4860,1.5267]	
Corners	[2.486,1.5210]	[2.486,1.5332]
	[2.532,1.5332]	[2.532,1.5210]

Actual location of the second landmine (metal rectangle):

Parameter	Co-ordinates [x,y]	
Centroid	[3.0150, 1.4561]	
Corners	[2.992,1.4501]	[2.992,1.4641]
	[3.084,1.4641]	[3.084,1.4501]

Actual location of the third landmine (metal sphere):

Parameter	Co-ordinates [x,y]	
Centroid	[3.8660,1.4245]	
Corners	[3.843,1.4205]	[3.843,1.4276]
	[3.889,1.4276]	[3.889,1.4205]

CHAPTER 6

CONCLUSION AND FUTURE WORK

CONCLUSION AND FUTURE WORK

The numerical model of the GPR strictly adheres to the corresponding real earth conditions, to achieve the same FDTD method has been incorporated for simulation of electromagnetic waves. Further, the B-Scan output obtained from the numerical model and from the actual hardware will be tested and verified. When the B-Scan output is subjected to the proposed algorithm for clutter reduction, all possible clutter, antenna crosstalk, ground bounce, reflections, false targets and AWGN were successfully removed and the same can be inferred from the result section for the different simulated scenarios. Till now, the algorithm can remove ground bounce of flat surfaces only but the algorithm will be improved to work for undulated surfaces. The location and the dimension estimation of the landmine is exceptional. But, can be further enhanced by error approximation. Material identification of the landmine has been developed only for metal and plastic but a novel approach is required to identify any material which will be worked upon. Concluding, the numerical model and the proposed algorithm succeed in localizing the landmine in any given realistic scenario.

REFERENCES

REFERENCES

[1] Antonios Giannopoulos "The Investigation of Transmission-Line Matrix and Finite-Difference Time-Domain Methods for the Forward Problem of Ground Probing Radar" PhD Thesis, The University of York, 1997.

[2] Craig Warren "Numerical Modelling of High-Frequency Ground-Penetrating Radar Antennas" PhD Thesis, The University of Edinburgh,2009.

[3] Nectaria Diamanti "An efficient ground penetrating radar finite-difference time-domain subgridding scheme and its application to the non-destructive testing of masonry arch bridges" PhD Thesis,The University of Edinburgh,2008.

[4] Iraklis Giannakis, Antonios Giannopoulos, Craig Warren "A Realistic FDTD Numerical Modeling Framework of Ground Penetrating Radar for Landmine Detection"IEEE Journal of Selected Topics in Applied Earth Observations and Remote Sensing (Volume:9 , Issue: 1), 28 August 2015.

[5] Claudio Bruschini, Bertrand Gros), Fre´de´ric Guerne, Pierre-Yves Piece, Olivier CarmonaLAMI-DeTeC, "Ground penetrating radar and imaging metal detector for antipersonnel mine detection",Journal of Applied Geophysics 40,ELSEVIER,31 October 1997.

[6] F. L. Teixeira, Weng Cho Chew, Fellow, IEEE, M. Straka, M. L. Oristaglio, Member, IEEE, and T. Wang ,"Finite-Difference Time-Domain Simulation of Ground Penetrating Radar on Dispersive, Inhomogeneous, and Conductive Soils" IEEE TRANSACTIONS ON GEOSCIENCE AND REMOTE SENSING, VOL. 36, NO. 6, NOVEMBER 1998.

[7] Andria van der Merwe and Inder J. Gupta, "A Novel Signal Processing Technique for Clutter Reduction in GPR Measurements of Small, Shallow Land Mines" ,IEEE TRANSACTIONS ON GEOSCIENCE AND REMOTE SENSING, VOL. 38, NO. 6, NOVEMBER 2000.

[8] Václav KABOUREK, Petr ČERNÝ, Miloš MAZÁNEK ,"Clutter Reduction Based on Principle Component Analysis Technique for Hidden Objects Detection", RADIOENGINEERING, VOL. 21, NO. 1, APRIL 2012.

[9] SATOSHI SUZUKI, KEIICHI ABE, "Topological Structural Analysis of Digitized Binary Images by Border Following", COMPUTER VISION, GRAPHICS, AND IMAGE PROCESSING N,32-46 (1985).